

Pressure Loss Associated with Flow Area Change in Micro-Channels

**A Thesis
Presented to
The Academic Faculty**

By

Toufik Y. Chalfi

**In Partial Fulfillment
Of the Requirements for the degree
Master of Science in Mechanical Engineering**

Georgia Institute of Technology

August 2007

Pressure Loss Associated with Flow Area Change in Micro-Channels

Approved:

S. Mostafa Ghiaasiaan, Chairman
School of Mechanical Engineering
Georgia Institute of Technology

Sheldon M. Jeter
School of Mechanical Engineering
Georgia Institute of Technology

Marc K. Smith
School of Mechanical Engineering
Georgia Institute of Technology

Approved Date

ACKNOWLEDGMENTS

First and foremost, I wish to thank my advisor Dr. S. M. Ghiaasiaan for his help, assistance, encouragement and precious advises throughout my work on this thesis. I would also thank my committee members Dr. S. Jeter and Dr. M. Smith for their time and consideration.

I also wish to express my gratitude to my dear parents Mr. M. Chalfi and Mrs. R. Chalfi for their continuous encouragement and support during my thesis and throughout my entire education.

I would also like to recognize my colleague graduate students in the School of Mechanical Engineering for their help and motivation especially Farooq Akram from the School of Aerospace Engineering.

TABLE OF CONTENTS

LISTE OF TABLES	vii
LISTE OF FIGURES	viii
NOMENCLATURE	x
SUMMARY	xii
1 INTRODUCTION	1
I.1. Scientific stakes of microfluidic systems	2
I.2 Characteristics and the validity of continuum representation of fluids	4
2 BACKGROUND AND LITERATURE SURVEY	8
2.1 General Remarks about Microchannels	8
2.1.1 What is Microchannel	9
2.2 Past experimental observation dealing with single-phase flow	10
2.3 Two-phase pressure drop in Microchannels	14
3 PRESSURE DROP IN FLOW AREA EXPANSION AND CONTRACTION	17
3.1 Single phase flow	17

3.2 Two-phase flow	20
4 EXPERIMENTAL APPARATUS AND PROCEDURE	24
4.1 Apparatus	24
4.2 Measurement and Procedures	25
4.3 Uncertainty	30
5 RESULTS AND DISCUSSION	34
5.1 Single-Phase Flow	34
5.1.1 Single-Phase Flow with Gas	34
5.1.2 Single-Phase Flow with Liquid	40
5.1.3 Correlation of the Data	41
5.2 Two-Phase flow, Flow Area Expansion	46
5.3 Two-Phase flow, Flow Area Contraction	55
6 CONCLUDING REMARKS	63
6.1 Conclusion	63
6.2 Recommendation for future research	65

APPENDICES

66

Appendix A: Data

BIBLIOGRAPHY

LIST OF TABLES

Table 2.1	Summary of potential research area related to microchannels	13
Table 4.1	Experimental loop instrumentation	25
Table 4.2	Uncertainties table	31
Table 5.1	Single-phase flow through sudden expansion-Experimental data for air	35
Table 5.2	Single-phase flow through sudden contraction-Experimental data for air	35
Table 5.3	Single-phase flow through sudden expansion- Experimental data for water	46
Table 5.4	Single-phase flow through sudden contraction-Experimental data for water	46
Table 5.5	Two-phase flow through sudden expansion-Experimental data	55
Table 5.6	Two-phase flow through sudden contraction-Experimental data	57

LIST OF FIGURES

Figure 1.1	Microscopic characteristic of a di-atomic gas and water liquid under normal conditions	4
Figure 2.1	Comparison of currently available experimental data	11
Figure 2.2	Schematic representation of various effects in micro-scale fully developed fluid flow	12
Figure 3.1	Pressure variation due to abrupt flow area changes	17
Figure 4.1	Schematic of the experimental set-up	24
Figure 4.2	Pressure drop measurements in the microchannel test section	26
Figure 4.3	Micro-channel cross section	26
Figure 4.4	Pressure profile in a test with water-contraction	28
Figure 4.5	Pressure profile in a test with air-contraction	28
Figure 4.6	Pressure profile in test with water-expansion	29
Figure 4.7	Pressure profile in test with two-phase-expansion	29
Figure 4.8	Pressure profile in test with two-phase-contraction	30
Figure 4.8	Sources of errors	31

Figure 5.1	Loss coefficients for air-expansion	37
Figure 5.2	Loss coefficients for air-contraction	38
Figure 5.3	Repeatability in measuring the expansion coefficient	38
Figure 5.4	Comparison of the pressure data with theory (air-exp)	39
Figure 5.5	Comparison of the pressure data with theory (air-cont)	39
Figure 5.6	Loss coefficients for water-expansion	42
Figure 5.7	Comparison of the pressure data with theory (water-exp)	42
Figure 5.8	Loss coefficients for water-contraction	43
Figure 5.9	Comparison of the pressure data with theory (water-cont)	43
Figure 5.10	Loss coefficient data for air and water expansion	44
Figure 5.11	Loss coefficient data for air and water contraction	45
Figure 5.12 – 5.19	Two-phase expansion pressure drop	48 - 54
Figure 5.20 – 5.23	Two-phase contraction pressure drop with vena-contracta	58 - 60
Figure 5.24 – 5.27	Two-phase contraction pressure drop with no vena-contracta	61 - 63

NOMENCLATURE

A	flow area (m ²)
C _c	vena-contracta coefficient
D	diameter (m)
G	mass flux (kg/m ² s)
j	superficial velocity (m/s)
K	loss coefficient
k _B	boltzmann constant (1.381x10 ⁻²³ J/k)
k _d	momentum correction factor
Kn	Knudsen number
ℓ	mean free path of the molecules (m)
<i>m</i>	mass flow rate (g/s)
P	pressure (Pa)
Re	Reynolds number
S	slip ratio
T	temperature (K)
t	time (s)
u	velocity (m/s)
We	weber number
x	flow quality
X _M	Martinelli factor

Greek symbols

α	void fraction
β	kinetic energy correction factor
Φ	two-phase multiplier
μ	viscosity (kg/ms)

ρ	density (kg/m ³)
ρ', ρ''	fictitious mixture densities (kg/m ³)
σ	flow area contraction ratio
τ	viscous stress (N/m ²)

Subscripts

C	vena-contracta
c	contraction
e	expansion
G	gas
H	hydraulic
h	homogeneous
I	irreversible
L	liquid
LO	all-liquid
R	reversible
s	slip
1	smaller channel
2	flow area change
2,1	flow area change location, towards the smaller channel
2,3	flow area change location, towards the larger channel
3	larger channel

SUMMARY

Pressure drop across miniature-scale flow disturbances, including abrupt flow area changes, is an important source of error and confusion in the literature. Such pressure drops are frequently encountered in experiments, where they are often estimated using methods and correlations that have been developed based on experimental data obtained in conventional systems. However, physical arguments as well as the relatively few available experimental observations indicate that such pressure drops in microchannel systems are likely to be different than what is known about similar phenomena in conventional flow systems. Experimental data dealing with pressure drop associated with two-phase flow across abrupt flow area changes in microchannels are scarce, however, and the available data are insufficient for the development of reliable predictive methods.

In this investigation, experiments were conducted using a test section consisting of two capillaries, one with 0.84 mm, and the other with 1.6 mm inner diameters. A multitude of pressure transducer ports were installed along the two capillaries, and allowed for the measurement of the pressure gradients over the entire test section. The test section allowed for the measurement of frictional pressure gradients in the two straight channels, as well as pressure drops caused by the flow area expansion and contraction depending on the flow direction, for single-phase as well as two-phase flows. These measurements were performed over a wide range of parameters, using air as the gaseous phase, and room-temperature water as the liquid phase. The single-phase flow data were compared with existing conventional correlations, and with predictions of CFD simulations using the Fluent computer code.

Based on the experience obtained in this study, the following observations and suggestions are made:

1. Conventional one-dimensional flow theory was generally inadequate for the prediction of pressure losses associated with single-phase flow, for both flow area expansion and contraction.
2. The widely-used one-dimensional homogeneous-flow model was also completely inadequate for the prediction of two-phase pressure drops. The experimental data indicated the occurrence of significant velocity slip. The one-dimensional slip flow model along with empirical correlation for the slip ratio, however, could predict the experimental data well for both flow area expansion and contraction.
3. The data for two-phase flow through the sudden contraction suggest that the vena-contracta phenomena did not occur.

1 INTRODUCTION

Due to the rapid development of new fields such as microelectromechanical systems (MEMS) and micrototal analysis systems (μ -TAS), flows of fluids in microchannels have become of capital importance and considerable interest has been given to applied and fundamental research in order to understand the basic phenomena and flow characteristics at the micro-scale level.

A deep understanding of fluid flow in microchannels is crucial before new and efficient micropumps and microactuators can be fabricated and utilized. Flows in these devices are often through channels with cross-section area change, and channels with bends and bifurcations. A systematic study dealing with these different configurations will provide helpful insight into the flow physics. They will also provide vital information for the design and analysis of micro-fluidic devices.

Fluid flow through microchannels and micro-devices are in fact encountered in numerous situations such as cooling of electronic devices, compact heat exchangers, chemical processing, and small-sized refrigeration systems, and their use has spread to cover most of industrial, medical and bioengineering applications.

Effective design of the microchannel heat sinks requires fundamental understanding of the characteristics of heat transfer and fluid flow in microchannels, microstructures, and flow networks consisting of complex interconnections. At the early stage of the designs, the relationships of macroscale fluid flow and heat transfer can be employed. However, many experimental observations have shown that fluid flow and heat transfer behaviors in microchannels deviate significantly from those in macroscale channels. Thus, although in many situations the existing macroscale design and analysis methods may be sufficient at least for preliminary design purposes, the final design of mini and micro-flow systems needs to be refined based on more accurate prediction models and correlations.

Flow and heat transfer in mini and microchannels have been under intensive investigations for more than 15 years now. Various aspects of single-phase and two-phase flow hydrodynamics and heat transfer have been experimentally investigated, and in some cases modeled and/or correlated.

Useful reviews of mini and micro-channels literature can be found, among others, in Ghiaasiaan and Abdel-Khalik [1], and Kandlikar et al [2]. There is some inconsistency and disagreement among various authors with respects to some specific phenomena. These will be briefly discussed later. However, an area that has received surprisingly little attention in the past is the pressure losses caused by flow disturbances (minor losses) in mini and micro-channel systems. This is indeed surprising, given the obvious importance of these losses in miniature systems. By far, the only significant experimental study is the investigation by Abdelall et al [3]. That study, however, indicates that the minor pressure losses in miniature scale flow fields are very different from what macro-scale models and correlations predict. The experimental investigation of Abdelall et al [3] addressed a relatively narrow scope of parameters, and in view of its controversial outcome it needs further verification.

The current investigation is thus aimed at the experimental re-examination of the tests and the data of Abdelall et al [3], and the expansion of the scope and parameter range of their data. The experimental data of Abdelall et al [3] primarily deal with high flow rates ($870 \leq Re_{LO} \leq 12,960$, with Re_{LO} defined based on the smaller channel). The experimental data in the present investigation are focused on low flow rates ($410 \leq Re_{LO} \leq 1020$).

1.1 Scientific stakes of microfluidic systems

The discussion of microchannel flow should start with a review of the important scales for the miniaturization of flow fields, and the assessment of the relevance of macro-scale models and analytical methods to micro-flow. As far as the motion of particles in near-atmospheric gas is concerned, the micron length represents a state of transition between

conventional size level and particles where quantum phenomena take place. For particles whose characteristic size is considerably larger than a micron, the continuum-based laws are valid. For particles much smaller than $1\ \mu\text{m}$ in size, the continuum-based methods become questionable since the particle's physical size is now comparable to the gas molecular mean free path. Between these limits the laws that govern fluid mechanics and transfers need to be well defined. When we deal with liquids, the situation is different since inter-molecular distances in liquids are much shorter than the typical molecular mean free paths in gases. Figure 1.1 compares the microscopic and molecular characteristics of typical liquids and gases. For liquids, we can thus apply continuum-based methods for sub-micron particles.

Now, let us address the flow in microchannels. Fluid and heat flows in conventional channels are modeled using the principles of conservation of mass, momentum (Newton's second law), and energy (first law of thermodynamics). Fluid transport phenomena in these conventional devices are described by the well known continuum-based Navier-Stokes (N-S) equations subject to a number of initial and boundary conditions (the no velocity slip and the no temperature jump conditions at the fluid-solid interface).

There exist three fundamental assumptions in order for the N-S equations to be valid:

- The Newtonian framework of mechanics
- The continuum approximation
- Thermodynamic equilibrium or at least quasi-equilibrium condition at fluid-solid interphases

Now, the question is: can we use the N-S equations to describe flows in microchannels? The answer to this question is yes as long as the three previous assumptions are still valid, a violation of any one of these assumptions would invalidate the use of the N-S equations and alternative modeling is then needed. For common gases at atmospheric pressure or higher, channels with hydraulic diameters $\geq 10\ \mu\text{m}$ can be analyzed using the

N-S equations. Currently, therefore, fluid flows in microchannels and micromachined fluid systems (e.g., pumps and valves) are analyzed using Navier-Stokes equations. However, when a flow channel is small enough such that continuum is no longer strictly applicable to it, a number of publications indicate that flows on the microscale are different from that on the macroscale and consequently the Navier-Stokes equations are unable of describing some phenomena related to such flows especially near wall conditions.

1.2 Characteristics and the validity of continuum representation of fluids

In order to determine the limit of the conventional law that govern fluid mechanics, we need to compare the internal scale of simple liquids and gases to the characteristic length scale of micro fluidic systems. These physical sizes are shown in Figure 1.1.

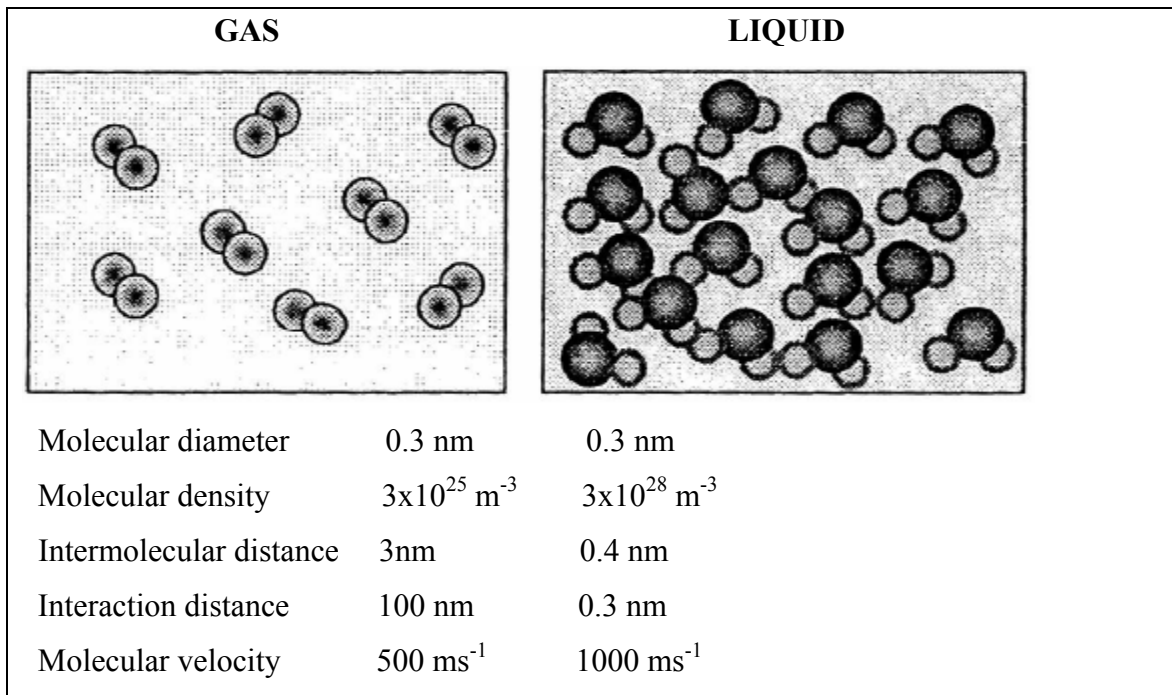


Figure 1.1 Microscopic characteristic of a di-atomic gas and water liquid under normal conditions

As noted, for gases as well as liquids, the molecular diameter and the intermolecular distance are considerably smaller than the size of microchannels of interest to this investigation.

The hydrodynamics and transport behavior of fluids in the continuum range are dictated by intermolecular collision. A brief discussion of the phenomena related to such collisions will therefore be presented now.

According to the kinetic theory of gases, the mean free path of the molecules λ is defined as the average distance traveled by a molecule before colliding with another molecule. This “grandeur” is a function of the density of the gas considered. In simple gas kinetic theory, where the molecules are idealized as rigid and spherical, for an ideal gas, it can be shown that

$$\lambda = \frac{k_B T}{\sigma P} \quad (1-1)$$

where P is the pressure, σ is the cross section area of the molecule, and k_B is the Boltzmann constant. For a gas of molecular diameter of 0.3 nm under normal conditions this expression gives λ equal to 140 nm.

Liquids possess microscopic characteristics which lay between the periodic well organized atoms of crystal, and gases which represent a dilute set of molecules. The study of such fluids is very complex and the models trying to describe such phenomena present a synthesis between a solid disorganized structure and a very dense gaseous medium [4]. In Eyring’s model, which is described by Bird et al. [5], liquid molecules are permanently moving and colliding with each other. This and other similar models imply a very small and almost insignificant distance between collisions. Therefore a more sophisticated theory is strongly needed in order to fully understand and quantify these phenomena.

As far as the validity of the continuum-based modeling is concerned, one should bear in mind that continuum applies when intermolecular collisions, and not molecule-wall interactions, determine the behavior of the fluid. Thus, evidently continuum applies when the molecular mean free path in gases (or intermolecular distance for liquids) is much shorter than the characteristic dimension of the flow channel. Consequently, for gases, we can define the Knudsen number as:

$$\text{Kn} = \lambda/L \quad (1-2)$$

where, L is the characteristic length scale of the considered system. We can then apply the following widely-used categories:

- $\text{Kn} < 10^{-3}$: Continuum regime: The Navier- Stokes equations are valid along with the no-slip condition at the wall. Thermal equilibrium is also applicable at the gas-solid interphase.
- $10^{-3} < \text{Kn} < 10^{-1}$: Slip regime: The Navier-Stokes equations are valid, however velocity slip and temperature jump at the gas-solid interface must be included.
- $10^{-1} < \text{Kn} < 10$: Transient flow regime: In this regime molecule-molecule collisions and molecule-wall interactions are both important.
- $10 < \text{Kn}$: Free molecular flow regime: In this regime intermolecular collisions are negligible. The molecules move ballistically.

For liquids, the Knudsen number does not apply. In order to define the limit of applicability of the continuum-based transport phenomena equations, we need to compare the characteristic time of mechanical solicitation to the molecular time response. According to [6], the Newtonian behavior of a liquid is valid when the velocity gradient is at least twice larger than the molecular characteristic frequency of liquids:

$$\left| \vec{\nabla}(u) \right| \leq 2(\tau_{molecular})^{-1} \quad (1-3)$$

For liquid water, the molecular characteristic time, calculated from molecular dynamic simulations [6], is about 10^{-12} s. These velocity gradient thresholds are not reached in microchannels, and the Newtonian behavior applies.

The evaluation of the macroscopic behavior of a liquid based on the molecular scale phenomena is very complicated and difficult, and experimental studies become very interesting and challenging. Investigations addressing the macroscopic liquid flow phenomena in microchannels are numerous, however. Also, several other phenomena can affect the experimental data for liquid flow in metallic microchannels. Included among them are the electrostatic interactions which take place at the wall.

2 BACKGROUND AND LITERATURE SURVEY

2.1 General remarks about microchannels

The rapid development of high-density power electronics has led to remarkably challenging thermal issues. Over the past several decades, transistor development has followed Moore's Law, which states that device sizes decrease exponentially over time [7]. Although advanced power semiconductor technologies have to some extent delayed the need for aggressive cooling by several years, the heat flux from the power device has risen significantly, approaching 500 W/cm^2 . This power level is beyond the capability of conventional heat sinks that are now used for silicon-based devices, which can achieve only about 20 W/cm^2 when maintaining junction temperatures below $150 \text{ }^\circ\text{C}$. Therefore, novel technologies must be developed for thermal management. The most promising technologies are based on microchannel cooling.

Also, the rapid development and wide application of high performance very large-scale integration (VLSI) technology result in significant improvement in the performance of electronic and microelectronic devices. However, with the augmentation of circuit density and operating speed, more heat is produced by the system. Since most operating parameters of the components are related to their temperature, thermal management of high power density electronic systems has become a very important aspect in electronic industry. Cooling those spots and removing total heat from the system present tremendous challenges to the system designer. Microchannel heat exchangers or microchannel heat sinks may provide efficient cooling for these high power density applications.

A flurry of research about microchannels has been undertaken around the world in the last decade and a half, with numerous studies each year. Ironically enough, most of the surprising results that were reported earlier were later attributed to experimental errors or faulty assumptions [8, 9, 10], but this fact did not quell the renewed focus on

microchannels. The latter references indicate that laminar flow theory agrees well with microchannel data. However, reported differences in turbulent flow have not been resolved. Furthermore, for two-phase flow as well as phase-change phenomena, microchannels do behave differently than conventional channels, because the relative magnitudes of frictional, gravitational and surface tension forces are scale-sensitive. Regardless of these academic pursuits, microchannels are thus bound to become more prominent once again due to Moore's Law.

2.1.1 What is a Micro-channel

The term micro-channel is often applied to channels whose hydraulic diameter lies in the 50 μ m to 1.5mm range. This size range is evidently too wide. Finer definitions also exist. Ghiaasiaan and Abdel-Khalik [1] have suggested that the threshold for the applicability of macro-scale two-phase flow models is:

$$D_H \geq 0.3 \sqrt{\frac{\sigma}{g\Delta\rho}} \quad (2.1)$$

Thus, channels with hydraulic diameters less than $0.3 \sqrt{\frac{\sigma}{g\Delta\rho}}$ are of interest to this study. For air/water like pairs, we thus are interested in the range $0.1 \text{ mm} \leq D_H \leq 1 \text{ mm}$. Today, these micro-channels are fabricated using several methods, some of the most common fabrication methods include bulk substrate etching and surface micro-machining. Micro-channels heat sinks have thus emerged as one of the effective cooling techniques. Fine channels, etched into a silicon wafer are built with a very high aspect ratio to increase their total surface area. As fluid flows through the microchannels, their large surface area enables them to cool hot spots as with temperatures as high as 1000 W/cm².

As mentioned earlier, in recent years, with the rapid progress in Micro-Electro-Mechanical-Systems (MEMS), many micromachining methods have been developed to

build micro-devices such as micro-motors, micro-sensors, micro-valves, micro-rockets, micro-gas-turbines,... etc. Microchannels as a means of cooling integrated circuits have been theorized since 1981, when Stanford professors David Tuckerman and Fabian Pease [11] published research proving that microchannels etched into silicon could remove heat densities as high as 1300 W/cm^2 while maintaining a temperature difference of less than $70 \text{ }^\circ\text{C}$.

There are two reasons for the efficiency of the microchannel heat exchangers. First, the heat generated by the chip travels a relatively small distance from the transistors on the chip, where the heat is generated, to the walls of the microchannels. Second, the heat from the walls of the microchannels conducts a very small distance into the fluid before the heat energy is carried away. As the microchannels get narrower, the walls of the channels stay cooler. Thus compared with conventional heat-exchangers, the main advantage of micro-heat-exchangers is their extremely high heat transfer area per unit of volume, and very large heat transfer coefficients, the overall heat transfer coefficient per unit volume can be greater than $100(\text{MW/m}^3\text{K})$, and miniaturization of devices and integration with complementary metal oxide semiconductors (CMOS) technology promise even better performance.

The compactness and high surface-to-volume ratios of micro scale fluid devices thus make them attractive alternatives to the conventional flow systems for heat transfer enhancement in numerous applications.

2.2 Past experimental observation dealing with single-phase flow

Table 2.1 summarizes some of the significant investigations that have been conducted on microchannel flows. Macro flow fields associated with separation and reattachment have received significant interest because of their importance in many engineering application [12]. But, due to the complicated nature of the phenomenon, similar studies in microchannels are yet to be carried out. At present, it is still difficult to conduct flow

visualizations in microsystems, and measurement of the pressure distribution along the channel is the only alternatives to investigate the flow pattern.

The normalized friction coefficient C^* ($C^* = (f.Re)_{exp}/(f.Re)_{theo}$) data as a function of the Reynolds number [13] are presented in Figure 2.1. The data are inconsistent and appear to be either greater or less than the theoretical prediction.

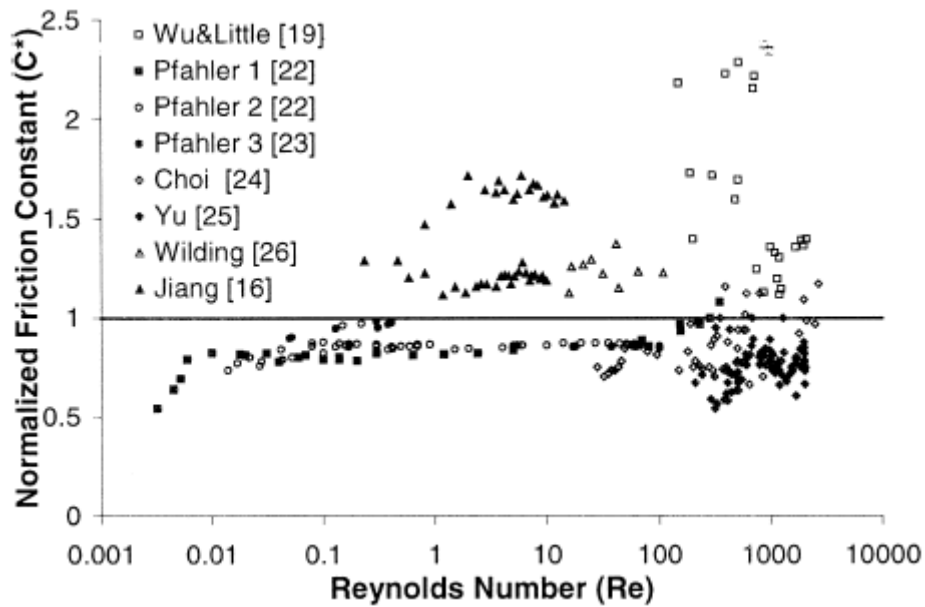


Figure 2.1 Comparison of the currently available experimental data [14]

Other issues that are important on the microscale are the surface effects, including variations of viscosity, slip velocity, temperature jump, and capillary effects. While some of these effects like slip velocity and temperature jump can be accounted for using the Navier-Stokes and Energy equations, other effects are yet to be accounted for, see Figure 2.2.

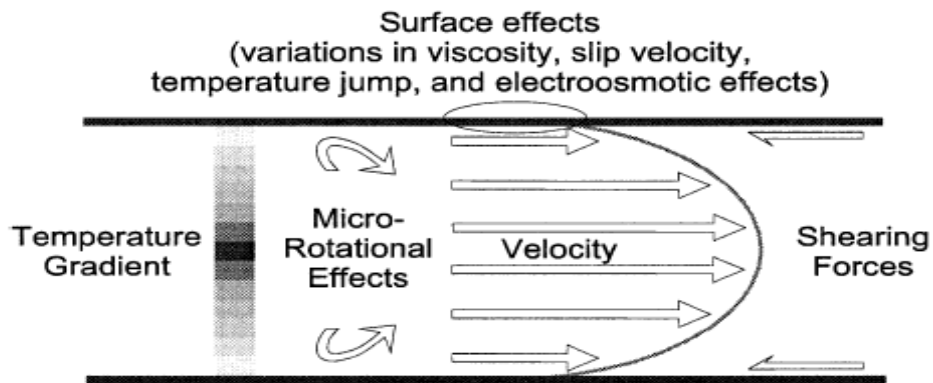


Figure 2.2 Schematic representation of various effects in micro-scale fully developed fluid flow [14]

Also other phenomena like viscous dissipation should not be underestimated in microchannels. W. Urbanck et al [15] reported that when water temperature raises from 300 to 310 K due to viscous dissipation, the kinematic viscosity decreases by 20% which results in a 25% increase of the local Reynolds number. Thus fluid temperature changes caused by viscous dissipation in microchannels may affect the friction factor and hence all transport phenomena.

Jadi et al [16] observed measurable liquid flow temperature rises (e.g, 6.2 K for iso-propanol in a long square fused-silica channel of 74.1 μm diameter for $\text{Re} = 300$) and related this to viscous dissipation. They suggested that the viscosity changes due to temperature changes should be taken into account to estimate the friction factor.

Table 2.1

Summary of potential research area related to microfluidic systems. [17]

General area and related studies	Potential research area
<p>1. <u>Characteristics of flow in microchannels</u></p> <p>(a) Microchannel cross-section [8,19]</p> <p>(b) Entrance effects [33]</p> <p>(c) Friction factor and pressure drop [16,20,34]</p> <p>(d) Surface roughness [63]</p> <p>(e) Joule heating [22,46,49]</p> <p>(f) Viscous dissipation [51,52]</p> <p>(g) Materials [5, 14, 17]</p>	<p>Triangular, elliptical, and non-uniform cross-section</p> <p>Analysis for smaller channels, Entrance effects on flow control</p> <p>Contradictions among various investigations and establishing some benchmark studies</p> <p>Effects of surface heterogeneity and defects</p> <p>Temperature effects on electro-osmotic flow profiles</p> <p>Viscous dissipation effects in fluids other than water</p> <p>Fabrication methods, cost reduction criterion. Use of flexible material</p>
<p>2. <u>Flow control in microchannels</u></p> <p>(a) Flow control and separation [4,37]</p> <p>(b) Flow mixing [4,41]</p>	<p>Leaks in microfluidic valves. Low separation efficiencies</p> <p>Enhancing mixing at micro scales, modeling of active mixtures</p>

2.3 Two-Phase pressure drop in Microchannels

The optimal safe function of many processes requires the assessment of the two-phase pressure drop associated with area enlargements, contractions, orifices, inserts...etc. The total pressure drop in the flow of two-phase mixtures consists of losses from friction, acceleration and in local resistance. The pressure drop in local resistances can be a significant fraction of the total losses; consequently the error in calculating them in the case of two-phase flow can produce un-acceptable inaccuracy in calculated circulation in loop. In spite of this, the pressure drop from local resistances to the flow of two-phase mixtures have not been well studied. The existing methods of calculating the pressure loss in local restrictions and disturbances are in most cases in poor agreement with experimental data, thus the standard methods based on the homogenous model may yield results exceeding the experimental data

Singularities such as sudden flow area changes, bends, valves, etc. are widely present in thermohydraulic two-phase circuits and many other industrial and bioengineering applications. Despite the importance of a correct pressure drop estimation in certain cases, for example in natural-circulation circuits [18], the behavior of gas-liquid two-phase fluids flowing through singularities is still one of the least studied aspects of the fluid dynamics of such mixtures.

Most experiments on two-phase flow pressure drop referred to in the literature have been carried out with air/water and steam/water mixtures. Thus, the physical properties of the fluids were not systematically varied and, additionally, flow parameters like mass flow and area ratio have been changed only in minor ranges. As a result, the recalculation of measured pressure drops by using available models will lead to poor results. The equations differ mostly in the definition of the mixture density and a reliable model for calculating the contraction coefficient in two-phase flow is lacking.

Attou et al [19] presented a uniform approach for the evaluation of two-phase flow pressure drop through several types of singularities: sudden enlargement, sudden

contraction, and orifice. Local balance equations were first averaged over a finite control volume including the local singularity of the duct. A general formulation of the two-phase pressure drop through the local flow resistance was obtained. The study showed that, for flow through an orifice, dissipation losses upstream of the orifice can contribute significantly to the total loss in the case of low liquid superficial velocity and high area ratio, particularly for low pressure flows. It is well known however, that for single-phase flow the major part of the mechanical energy dissipation takes place in the expansion zone of the flow. In single-phase flows, dissipation is most often negligible in the contraction region; Attou's analysis thus shows that this may not be the case for two-phase flows.

The behavior of two-phase flow through a sudden expansion has been the subject of several experimental and theoretical investigations. The important parameter which characterizes this type of singularity is the global singular pressure variation. Several analytical methods of calculating this quantity exist in the literature [20-23]. A crucial piece of information is the void fraction. Some of these methods use an empirical correlation for void fraction, while others are incomplete and need closing relationships for the global void fraction.

Schmidt et al [24] developed a new model to calculate the two-phase pressure drop across a sudden contraction. From measurements of the location and size of the narrowest cross section in the pipe contractions it was concluded that unlike single-phase flow a two-phase flow does not contract behind the edge of the transition. Thus, the contraction coefficient associated with the venna-contracta phenomena seems at least in two-phase flow not to be an essential physical parameter and should, therefore, be used with caution.

Abdellah et al [3], however, showed that two-phase pressure drop caused by flow area expansion and contraction in mini and microchannels were significantly lower than the prediction of the homogeneous flow model, and thus indicated significant velocity slip in

the vicinity of the flow area change, and model prediction assuming a slip ratio of $S = (\rho_L / \rho_G)^{1/3}$ resulted in relatively good agreement between theory and data.

3 PRESSURE DROP IN FLOW AREA EXPANSION AND CONTRACTION

3.1 Single phase flow

In this chapter the experimental and analytical background related to the pressure changes caused by sudden flow area expansion and contraction will be reviewed in some detail.

Consider the system shown in Figure 3.1. When an incompressible fluid flows through a sudden expansion, the total and irreversible pressure drops can be evaluated by applying the one-dimensional momentum and mechanical energy conservation equations

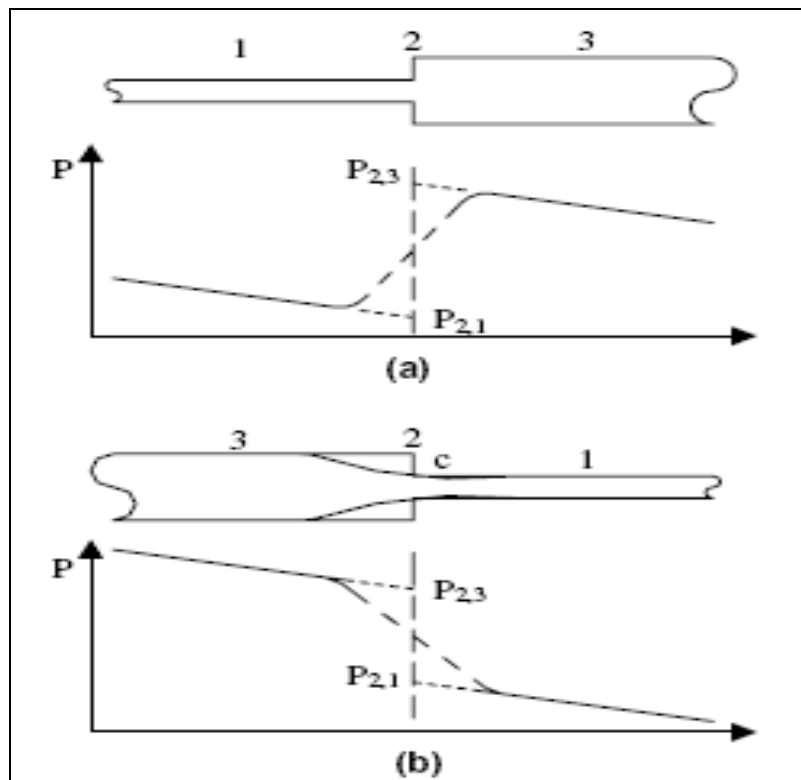


**Figure 3.1 Pressure variations due to abrupt flow area changes:
(a) sudden expansion (b) sudden contraction**

$$\begin{aligned}
\Delta P_e &= P_{2,1} - P_{2,3} = \Delta P_{e,R} + \Delta P_{e,I} \\
&= \rho_L \langle u_1 \rangle^2 (\sigma^2 k_{d3} - \sigma k_{d1})
\end{aligned} \tag{3.1}$$

with;

$$\Delta P_{e,I} = K_e \rho \frac{\langle u_1 \rangle^2}{2} \tag{3.2}$$

$$\Delta P_{e,R} = -\rho \frac{\langle u_1 \rangle^2}{2} (1 - \sigma^2) \tag{3.3}$$

Such that;

$$K_e = 1 - 2k_{d1}\sigma + \sigma^2(2k_{d3} - 1) \tag{3.4}$$

where,

$$\sigma = \frac{A_1}{A_3} \tag{3.5}$$

$$k_d = \frac{\langle u^2 \rangle}{\langle u \rangle^2} \tag{3.6}$$

For any property ξ , the flow area averaging is defined as;

$$\langle \xi \rangle = \frac{1}{A} \int_A \xi \, dA \tag{3.7}$$

Assuming a flat velocity profile, $k_{d1} = k_{d3} = 1$, Equation (3.4) reduces to the Borda-Carnot relation $K_e = (1 - \sigma)^2$.

Single-phase flow through a sudden contraction leads to the well-known vena-contracta phenomenon. For this case and up to the vena-contracta point C, the fluid acceleration is believed to be approximately isentropic, and mechanical energy loss takes place during the deceleration following the vena-contracta point. The expansion from the vena-contracta point to a developed flow can be modeled as flow through sudden expansion [25], and that leads to;

$$\begin{aligned} \Delta P_c &= P_{2,3} - P_{2,1} = \Delta P_{c,R} + \Delta P_{c,I} \\ &= \rho \frac{\langle u_1 \rangle^2}{2} \frac{1 - \beta_3 \sigma^2 C_c^2 - 2C_c + 2C_c^2 k_{d1}}{C_c^2} \end{aligned} \quad (3.8)$$

where;

$$\beta = \frac{\langle u^3 \rangle}{\langle u \rangle^3} \quad (3.9)$$

And from Geiger correlation [26]

$$C_c = 1 - \frac{1 - \sigma}{2.08(1 - \sigma) + 0.5371} \quad (3.10)$$

In driving Equation (3.8), a flat velocity profile at the vena-contracta cross-section has been assumed. Also by assuming a flat velocity profiles at the cross-section 3 and 1, Equation (3.7) reduces to

$$\Delta P_c = \rho \frac{\langle u_1 \rangle^2}{2} \left[\left(1 - \frac{1}{C_c} \right)^2 + 1 - \sigma^2 \right] \quad (3.11)$$

For laminar flow in circular channels, the parabolic velocity profile leads to $\beta = 2$ and $k_d = 1.33$. For fully turbulent flow, on the other hand, the velocity profile is approximately flat and $k_d \approx \beta \approx 1$.

3.2 Two-phase flow

Following an analysis similar to the analysis leading to Equation (3.1), the pressure change in a sudden expansion associated with two-phase flow without phase change, can be shown to be;

$$\Delta P_e = P_{2,1} - P_{2,3} = G_1^2 \sigma \left(\frac{\sigma}{\rho'_3} - \frac{1}{\rho'_1} \right) \quad (3.12)$$

where;

$$\rho' = \left[\frac{1 - x^2}{\rho_L(1 - \alpha)} + \frac{x^2}{\rho_G \alpha} \right]^{-1} \quad (3.13)$$

To estimate the reversible pressure drop, the following expression from [27] can be used,

$$\int_{P_{2,1}}^{P_{2,3}} \frac{dP}{\rho_h} \Big|_R = \frac{G_1^2}{2} \left(\frac{1}{\rho_3^{n_2}} - \frac{\sigma^2}{\rho_1^{n_2}} \right) \quad (3.14)$$

with;

$$\rho_h = \left(\frac{x}{\rho_G} + \frac{1-x}{\rho_L} \right)^{-1} \quad (3.15)$$

$$\rho'' = \left[\frac{(1-x)^3}{\rho_L^2(1-\alpha)^2} + \frac{x^3}{\rho_G^2\alpha^2} \right]^{-1/2} \quad (3.16)$$

In order to apply Equation (3.14), an empirical relation between α and x is needed, which means that the reversible pressure change cannot be obtained from pure theory. Consequently only the total two-phase pressure changes are usually modeled. When both liquid and gas phases are considered to be incompressible, and assuming that the void fraction remains unchanged across the flow disturbance, then;

$$\Delta P_e = \Phi_{LO,e} \Delta P_{LO,e} \quad (3.17)$$

where;

$$\Delta P_{LO,e} = \frac{G_1^2}{\rho_L} \sigma(\sigma - 1) \quad (3.18)$$

$$\Phi_{LO,e} = \frac{\rho_L}{\rho'} \quad (3.19)$$

$$\Delta P_{e,I} = \frac{G_1^2}{2\rho_L} \left[\frac{2\rho_L}{\rho'} \sigma(\sigma - 1) - \rho_h \frac{\rho_L}{\rho''^2} (\sigma - 1) \right] \quad (3.20)$$

Equations (3.17)-(3.20) are good for predicting experimental data in conventional channels [27, 28]. However, significant velocity slip occurs at both sides of the enlargement [29].

Two-phase flow across sudden contraction represents a more complicated and interesting process in comparison with a sudden enlargement. Most of the studies dealing with this flow situation assume the occurrence of the vena-contracta phenomenon [29, 33], and in analogy with single-phase flow, they have assumed that all dissipation effects take place downstream of the vena-contracta point. Following these assumptions, the total pressure loss across a sudden contraction can be represented as follow,

$$\begin{aligned} \Delta P_c &= P_{2,3} - P_{2,1} \\ &= G_1^2 \left\{ \frac{\bar{\rho}_h}{2} \left(\frac{1}{C_c^2 \rho_{2,1}''^2} - \frac{\sigma^2}{\rho_3''^2} \right) + \left(\frac{1}{\rho_1'} - \frac{C_c}{\rho_{2,1}'} \right) \right\} \end{aligned} \quad (3.21)$$

where $\bar{\rho}_h$ can be found using Equation (3.15), and utilizing parameters averaged between locations 2 and C. By considering incompressible liquid and gas phases, and assuming that α and x remain unchanged across the sudden contraction; Equation (3.21) reduces to,

$$\Delta P_c = G_1^2 \left\{ \frac{\rho_h}{2\rho''^2} \left(\frac{1}{C_c^2} - \sigma^2 \right) + \frac{1}{\rho'} (1 - C_c) \right\} \quad (3.22)$$

The homogeneous flow assumption is usually applied, based on the argument that effective mixing is caused by the sudden contraction [26, 27, 29, 30-34], which leads to

$$\Delta P_c = \Delta P_{LO,c} \Phi_{LO,c} \quad (3.23)$$

The total pressure change will then be:

$$\Delta P_{LO,c} = \frac{G_1^2}{2\rho_L} \left\{ \left(\frac{1}{C_c} - 1 \right)^2 + (1 - \sigma^2) \right\} \quad (3.24)$$

$$\Phi_{LO,c} = 1 + \frac{x(\rho_L - \rho_G)}{\rho_L} \quad (3.25)$$

This model is based on vena-contracta phenomenon; in other words, it assumes that for such systems, the vena-contracta in two-phase flows as well as single phases flows take place in the same location, and result in the same contraction ratio, C_c (see Equation 3.10).

4 EXPERIMENTAL APPARATUS AND PROCEDURE

4.1 Apparatus

Figure 4.1 shows the experimental apparatus used in this study. A rubber bladder within a steel tank is filled with water. Compressed gas from a regular cylinder is used to maintain a constant pressure in the steel tank; this assures that the water pressure and the flow rate are stable during an experiment. Compressed air is passed through a filter, regulated air line. The mass flow rate for both air and water are measured in a set of flowmeters calibrated to measure low and high flow rates.

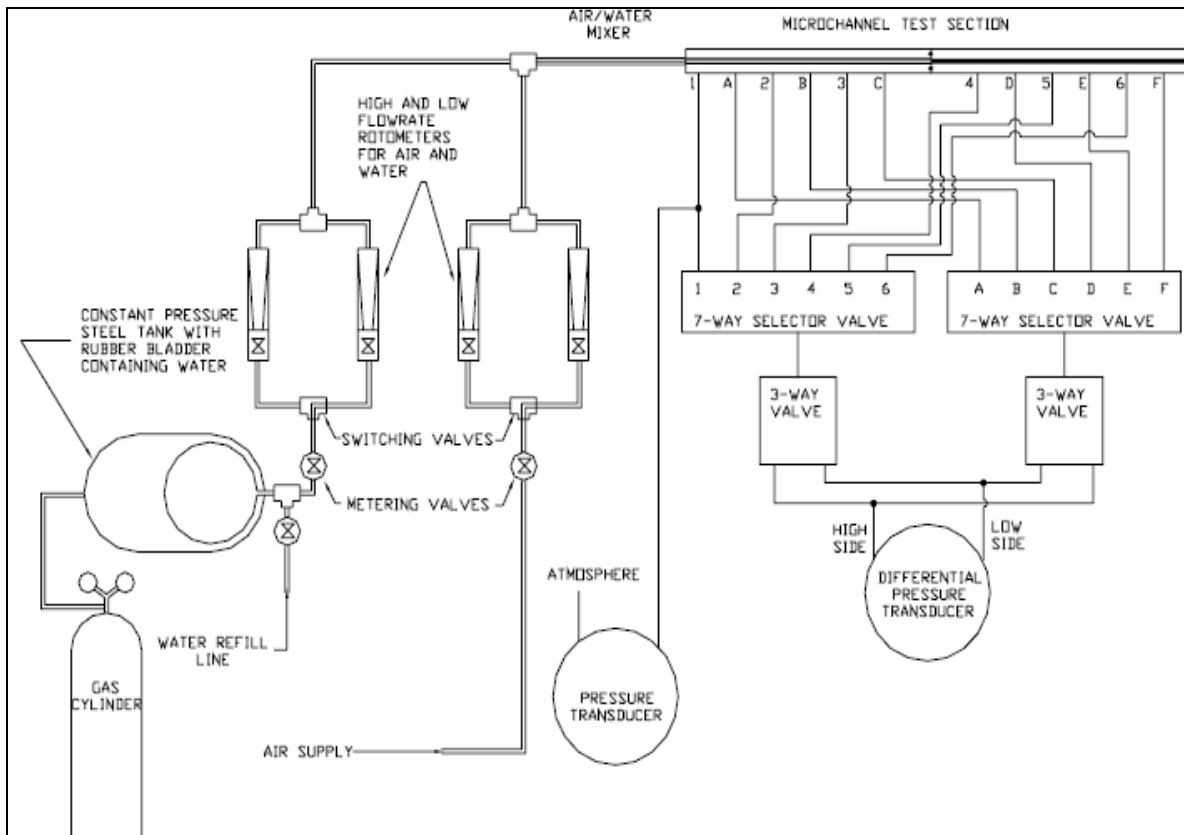


Figure4. 1 Schematic of the experimental set-up

The air and water streams meet in a tee fitting up-stream of a 4.8 mm diameter and 178 mm long static in line mixer directly connected to the test section. The test section is made from two abutting stainless steel tubes within a brass hosing for structural stability. The stainless steel tubes have 0.84 and 1.6 mm diameters, respectively, which produce a sudden area change, a sudden expansion or a sudden contraction depending on the flow direction. Figure 4.3 shows a cross- section of the test section where the two tubes meet up. The experimental instrumentation used in this investigation is summarized in Table 4.1

Table 4.1

Experimental loop instrumentation

Description	Manufacturer stated range	Manufacturer stated accuracy
Flow-meter, air	644-2217 cm ³ /min	2%
Flow-meter, water	0.44-20.90 cm ³ /min	2%
Differential pressure transducer	0-37.4 kPa	0.1% cal. Range
Differential pressure transducer	0-25 kPa	0.1% cal. Range
Total pressure transducer	0-186.8 kPa	0.1% cal. Range

4.2 Measurements and procedures

Figure 4.2 shows the pressure drop measurement system used in this study. Six pinholes of 0.5 mm diameter and located at 20 mm intervals serve as pressure taps for each tube. These clean and burr-free pinholes were created on the tube walls using precision electric discharge machining (EDM). A threaded hole with 8.6 mm diameter in the brass hosing is centered over each pinhole. The pressure taps “4” and “C” are located at 25 mm from the flow area change singularity.

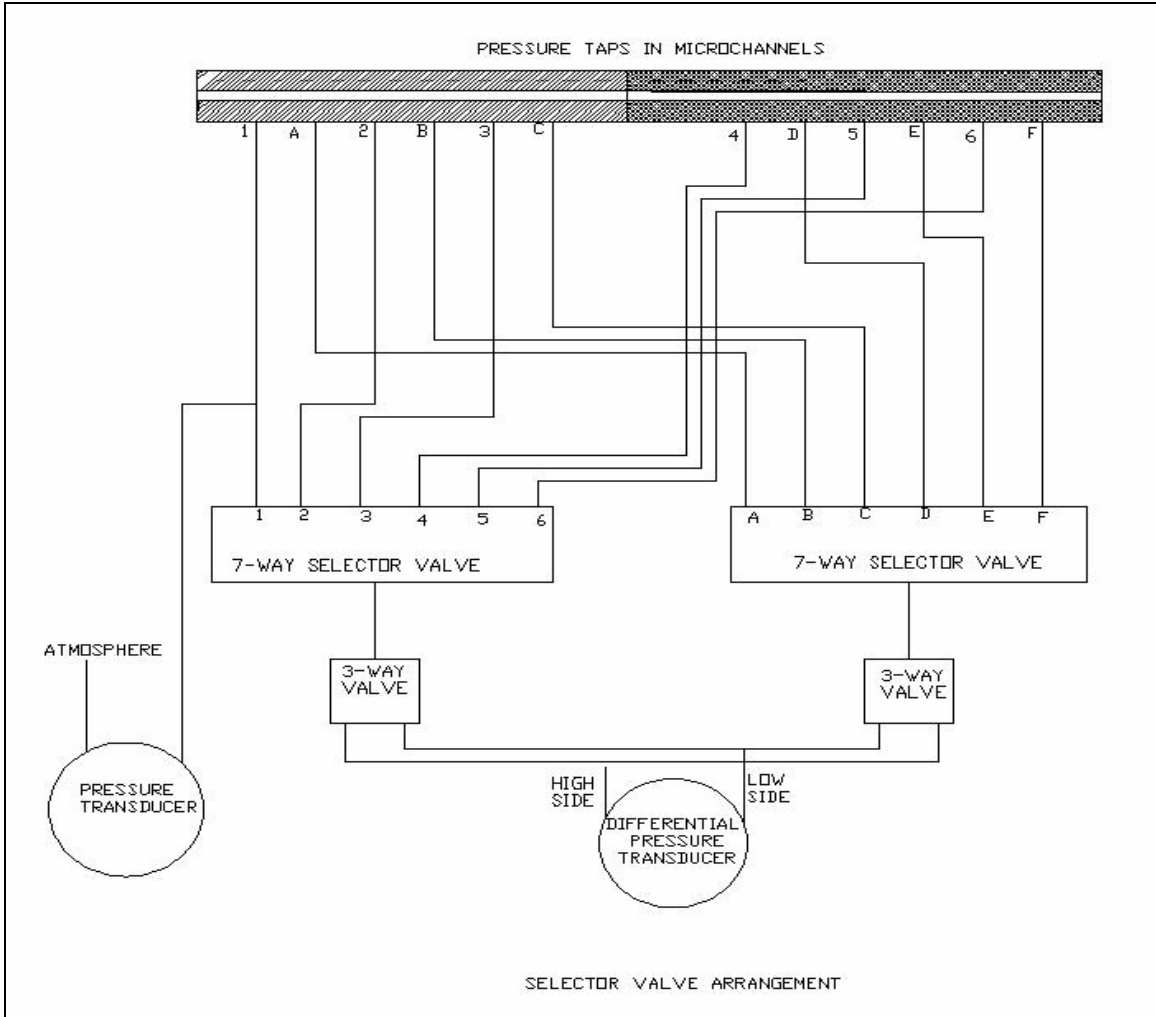


Figure 4.2 Pressure drop measurements in the micro-channel test section

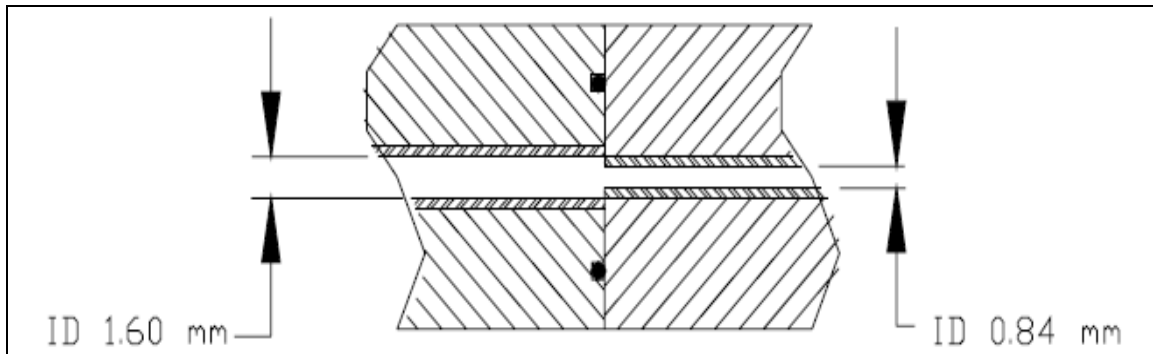


Figure 4.3 Micro-channel cross-section

The differential pressure measurements are done such that at any time only one pressure transducer is used; this eliminates cross-calibration errors. The pressure taps are connected to a 7-way selector valve with 3.2 mm ID plastic tubing, in turn the 7-way selector valve is connected to a 3-way selective valve, and finally the 3-way selector valve is connected to a differential pressure transducer. We obviously need the absolute pressure at least at one point. The absolute pressure at location 1 in Figure 4.2 is measured from a tee coming off from pressure tap 1 and connected to a separate pressure transducer. This transducer is calibrated to measure the absolute pressure at the first measurement point.

In order to maximize the accuracy of the measurements, three Rosemount 1151DP model pressure transducers were used, each calibrated for a different pressure range. The ranges of these transducers are 0-6.25, 0-37.4, and 0-186.8 kPa. The accuracy of each transducer is about $\pm 0.1\%$ of its span, and the accuracy of the liquid and gas volumetric flow rate is $\pm 2\%$.

Each test was initiated by first verifying that all tubing lines were full of water and contained no trapped air bubbles. The mass flow rate of each fluid was then adjusted to its desired level using metering valves, and the system was allowed to reach steady state. The pressure drop between each adjacent pressure tap pairs was then measured by adjusting the selector valve setting and was recorded by an NI PCI-6220 data acquisition

system. By extrapolating the pressure profiles in the two stainless steel tubes, the total pressure change over the flow area change can be evaluated. Figures 4.4 through 4.8 display some examples of the measured pressure profiles.

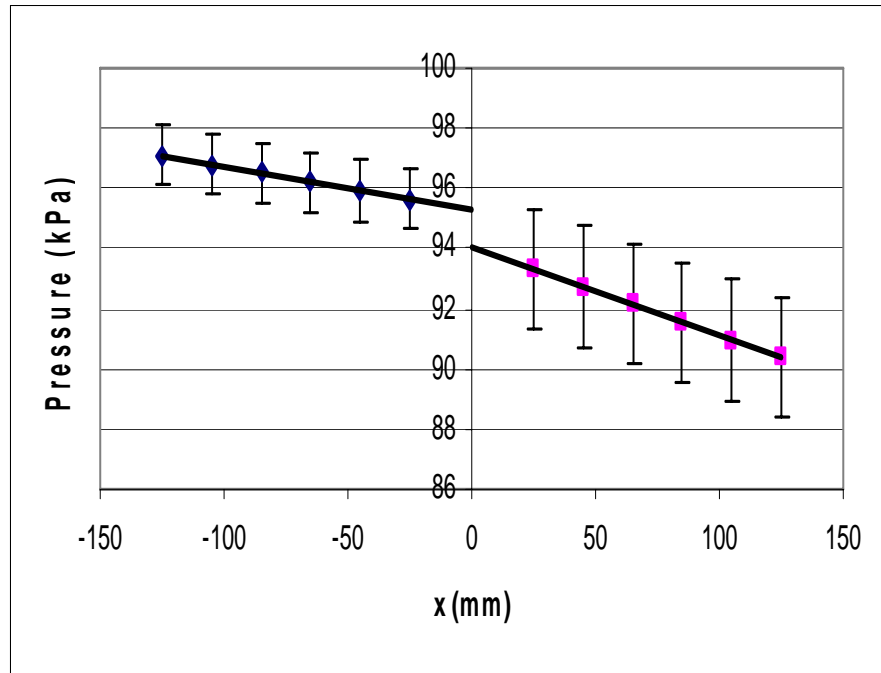


Figure 4.4 Pressure profiles in a test with water-contraction

$$\dot{m} = 0.1956 \text{ g/s}$$

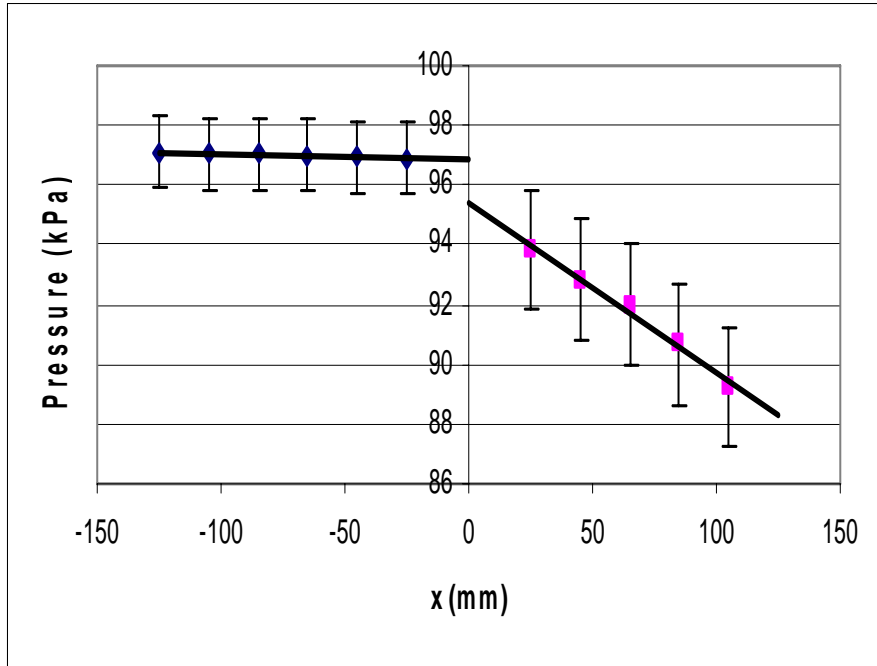


Figure 4.5 Pressure profiles in a test with air-contraction

$$\dot{m} = 0.746 \text{ g/s}$$

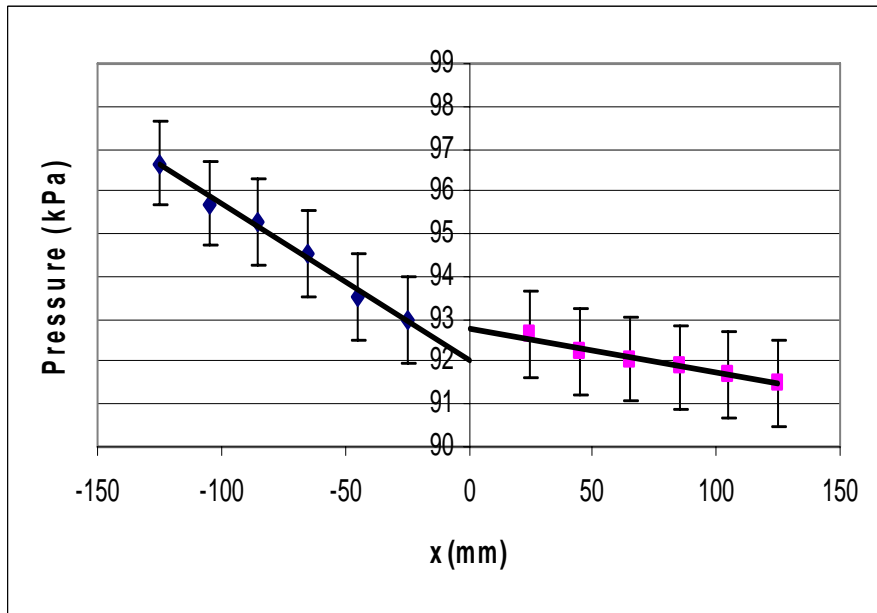


Figure 4.6 Pressure profiles in a test with water-expansion

$$\dot{m} = 0.2561 \text{ g/s}$$

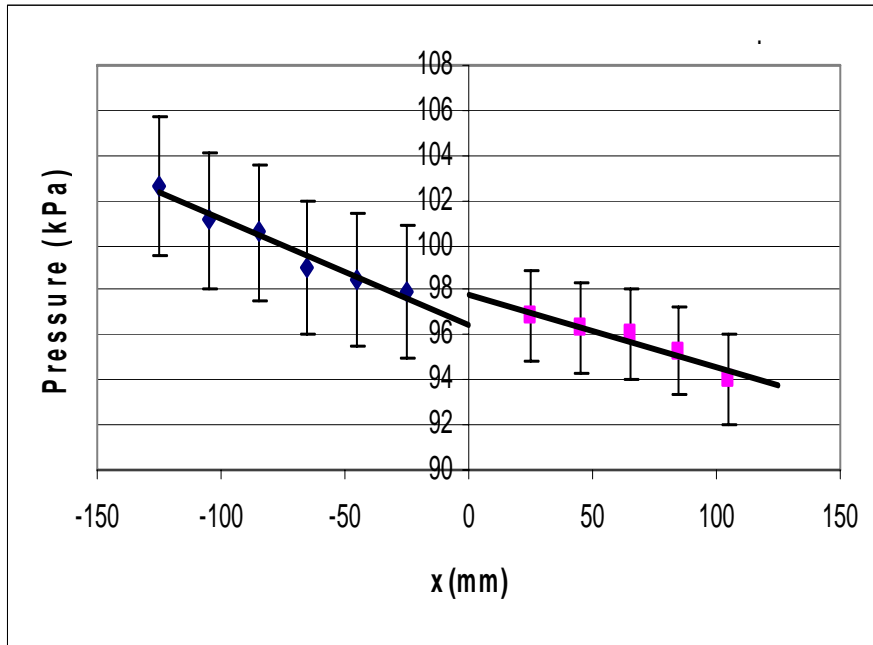


Figure 4.7 Pressure profiles in a test with two-phase-expansion

$$\dot{m}_L = 0.2865 \text{ g/s} \quad \dot{m}_G = 0.0171 \text{ g/s}$$

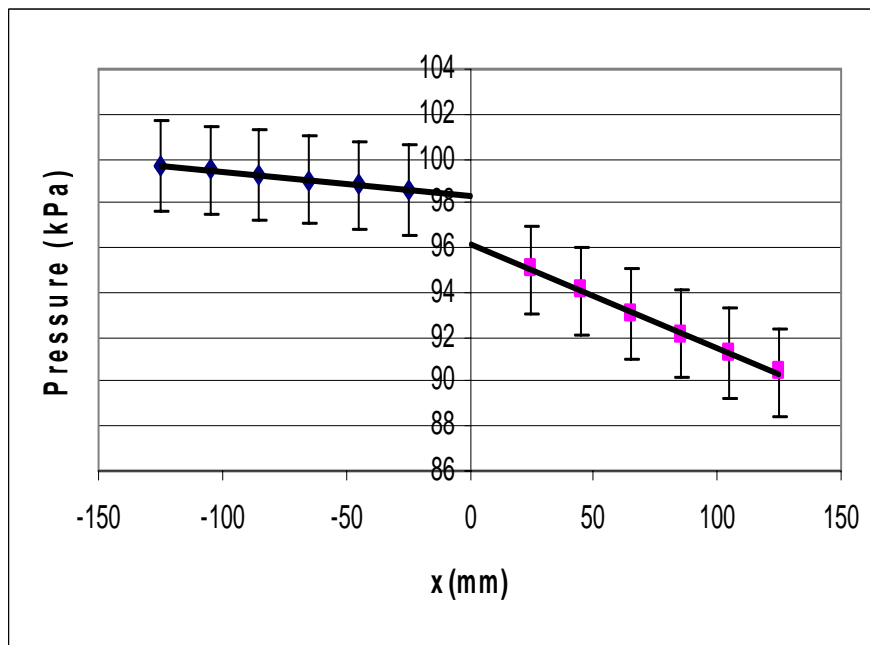


Figure 4.8 Pressure profiles in a test with two-phase-contraction

$$\dot{m}_L = 0.2561 \text{ g/s} \quad \dot{m}_G = 0.0139 \text{ g/s}$$

4.3 Uncertainty

In any experimental work it is very important to evaluate and quantify all the major sources of errors that can affect the measurements. These errors are usually due to instrumentation, data acquisition, facility and environmental effects. Experimental uncertainty estimates are imperative for risk assessments in design both when using data directly or in calibrating and validating simulation methods.

The accuracy of a measurement indicates the closeness of agreement between an experimentally determined value of a quantity and the true value. In practice, the true values of measured quantities are rarely known. Thus, one must estimate error, and that estimate is called an uncertainty, U . Figure 4.9 illustrates this concept.

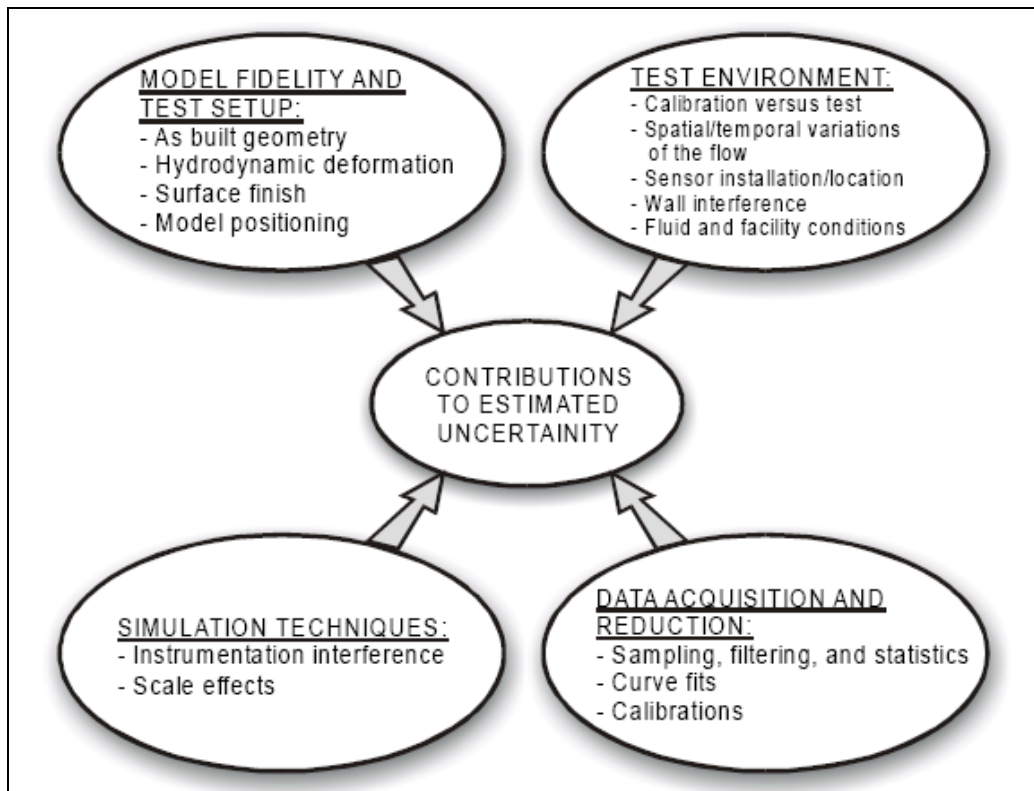


Figure 4.9 Sources of errors (adapted from AIAA, 1995)

In measuring the pressure drop in this study, care was taken to make the measurement as accurate and reliable as possible. The possible sources of error can be related to the flow-meters which were used for measuring the mass flow rates for both air and water in the micro-channel test section, and the pressure transducers which were used to convert the pressure into voltage for analysis using a data acquisition system. Noise effects were also taken into account by using a low pass filter to eliminate high frequency fluctuations. The transducers were all re-calibrated before each experiment to make sure that they were working properly. The following table summarizes all the instrumental uncertainties, where U_A represents the uncertainty associated with measurement random error, and U_B stands for the uncertainty associated with the accuracy of the measurement device. (U_B is often provided by the manufacturer).

Table 4.2:
Uncertainties table

Generic ID	Commercial ID	U_A	U_B
Flow-meter, air	Brooks instruments Tube # R-225-B	2.05cm ³ /min	2% cal. range
Flow-meter, water	Brooks instruments Tube # R-215-D	0.022cm ³ /min	2% cal. range
Data-acquisition System	National instrument NI-PCI 6220	NA	NA
differential pressure transducer	Rosemount. Inc 1151 DP	NA	0.1% cal. range
Total-Pressure transducer	Rosemount. Inc 1151 DP	NA	0.1% cal. range

The combined uncertainty of the measurement can be estimated using the following equation:

$$U_C = \sqrt{(U_A^2 + U_B^2)} \quad (4.1)$$

In dealing with the measurement of the pressure, one notes that the total uncertainty is the resultant of the errors associated with each instrument. Then, based on the information related to the expected source of errors, an error propagation analysis (EPA) related to the calculation of the loss coefficient (Equation 5.1) can be done using the following equation:

$$U_K = \sqrt{\left(\frac{\partial k}{\partial u_1} U_{c1}\right)^2 + \left(\frac{\partial k}{\partial P} U_{c2}\right)^2} \quad (4.2)$$

with;

$$\frac{\partial k}{\partial u_1} = (\sigma^2 - 1)$$

$$\frac{\partial k}{\partial P} = 1$$

and U_{c1} and U_{c2} are the total pressure uncertainties related to the flow-meter and pressure transducers respectively.

5 RESULTS AND DISCUSSION

5.1 Single-Phase Flow

5.1.1 Single-Phase Flow with Gas

Tables 5.1-5.2 summarize the experimental data obtained for air. The loss coefficient in this study is calculated based on the measured pressure drops assuming a uniform velocity profile ($k_d = \beta = 1$) both at inlet and outlet. Consequently, for a sudden expansion we have (see Figure 4.3):

$$K_e \left(\frac{1}{2} \rho \langle u_1 \rangle^2 \right) = (P_{2,1} - P_{2,3}) - \frac{1}{2} \rho \langle u_1 \rangle^2 (\sigma^2 - 1) \quad (5.1)$$

where $(P_{2,1} - P_{2,3})$ is obtained experimentally. For the sudden contraction case the same Equation (5.1) can be used replacing K_e with K_c , and changing the signs of both terms on the right hand side.

The Reynolds number here and everywhere else is always defined based on the smaller channel. The experimental data are each in fact the averages of several tests where repeatability of experiments were tested.

Table 5.1

Single-phase flow through sudden expansion-Experimental data for air.

\dot{m} (g/s)	Re	$P_{2,3}-P_{2,1}$ (kPa)	$K_e(\text{exp})$	$K_e(\text{th})$
0.0243	1997	0.106	0.72	0.34
0.0377	3103	0.276	0.74	0.34
0.0505	4153	0.464	0.75	0.52
0.0630	5181	0.593	0.78	0.52
0.0746	6131	0.688	0.80	0.52
0.0846	6953	0.774	0.82	0.52
0.0937	7700	0.910	0.82	0.52
0.1023	8407	1.173	0.81	0.52
0.1099	9035	1.265	0.82	0.52
0.1196	9830	1.366	0.83	0.52
0.1266	10409	1.487	0.84	0.52
0.1338	11002	1.774	0.83	0.52

Table 5.2:

Single-phase flow through sudden contraction-Experimental data for air.

\dot{m} (g/s)	Re	$P_{2,3}-P_{2,1}$ (kPa)	$K_c(\text{exp})$	$K_c(\text{th})$
0.0377	3103	0.882	0.44	0.38
0.0505	4153	1.025	0.45	0.38
0.0630	5181	1.302	0.49	0.38
0.0746	6131	1.437	0.56	0.38
0.0846	6953	1.584	0.59	0.38
0.0937	7700	2.237	0.57	0.38
0.1023	8407	2.757	0.56	0.38
0.1099	9035	2.872	0.58	0.38
0.1196	9830	2.904	0.61	0.38
0.1266	10404	3.099	0.62	0.38
0.1338	11002	3.207	0.63	0.38

The loss coefficient data obtained for this case are shown in Figures 5.1 and 5.2 for sudden expansion and contraction cases, respectively. Figure 5.3 is similar to Figure 5.1. In Figure 5.3, however, measurements from three separate test series are shown. Figure 5.3 shows very good repeatability. The figure depicts three sets of data (series K_{e2} , K_{e3} and K_{e4}). The data points denoted with $K_e(\text{exp})$ and represented by a solid square are thus each the average of three measurements.

Some observation can be made. First, there has been excellent repeatability. Second, the data indicate that K_e is a weak function of Reynolds number. For $Re \geq 5,000$, in fact, the data can be represented with a constant $K_e = 0.80$. For $Re \leq 5,000$, a slight dependence on Re can be seen; nevertheless $K_e = 0.80$ can be considered a good approximation.

For the sudden expansion case, as noted in figure 5.1, the data conform to $K_e = 0.80$. The Borda-Carnot theory, however, predicts $K_e = (1 - \sigma)^2 \approx 0.52$. The data thus indicate consistently higher values than the Borda-Carnot relation.

Figure 5.4 depicts the sudden expansion data, this time the total measured pressure drop values are compared with Equation (3.1). However, $k_{d1} = 1.3$ and/or $k_{d3} = 1.3$ were used wherever laminar flow situation were encountered. As expected, Equation (3.1) disagrees with data, due to the small loss coefficient it represents. The predictions of the following equation are also shown in the Figure:

$$\Delta P_e = K_e \rho \frac{\langle u_1 \rangle^2}{2} - \rho \frac{\langle u_1 \rangle^2}{2} (1 - \sigma^2) \quad (5.2)$$

where now $K_e = 0.80$ is used. As noted, the predictions of the above equation agree with the experimental data.

Figure 5.2 shows that, for the sudden contraction case the data correlate well with $K_c = 0.56$. One again the experimental value of k_c is larger than the prediction of the

correlation of Geiger [26], whereby $K_c = (1 - 1/C_c)^2$ and C_c is found from Equation (3.10). The difference between the measured and predicted K_c is slight, however.

Figure 5.5 shows the same contraction pressure drop data, this time the total pressure change across the contraction is compared with Equation (3.8). Furthermore, wherever the flow was laminar at inlet, $k_{d1} = 1.3$ was used, as noted. Also, when the flow was laminar in both inlet and outlet, $k_{d1} = 1.3$ and $\beta = 2$ were assumed. As noted, the measured total pressure drops are only slightly higher than the theoretical prediction with Geiger's relation for K_c . When $K_c = 0.56$ is used, however, good agreement is seen between data and theory, as expected.

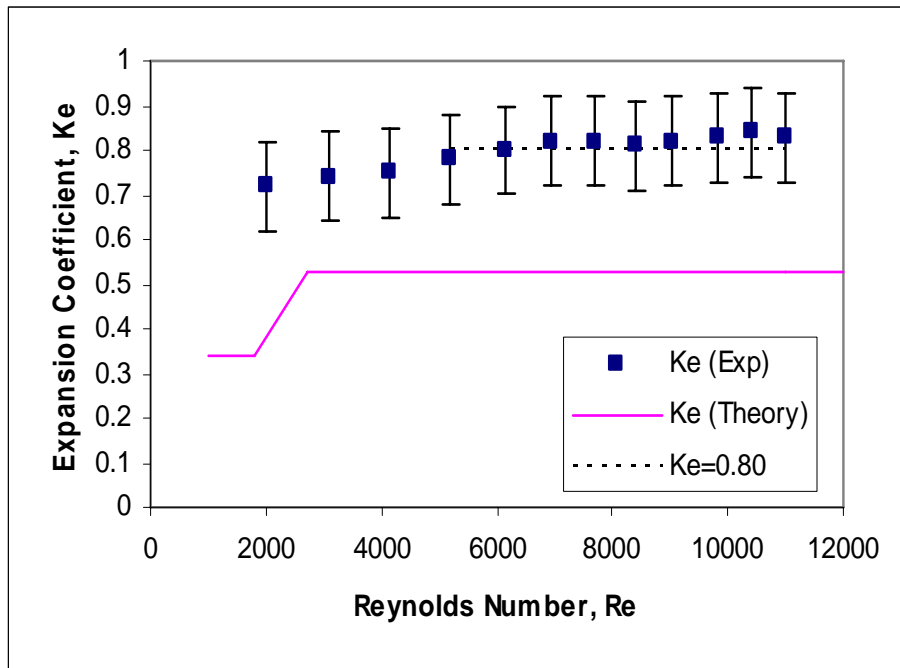


Figure 5.1 Loss coefficients for air-expansion

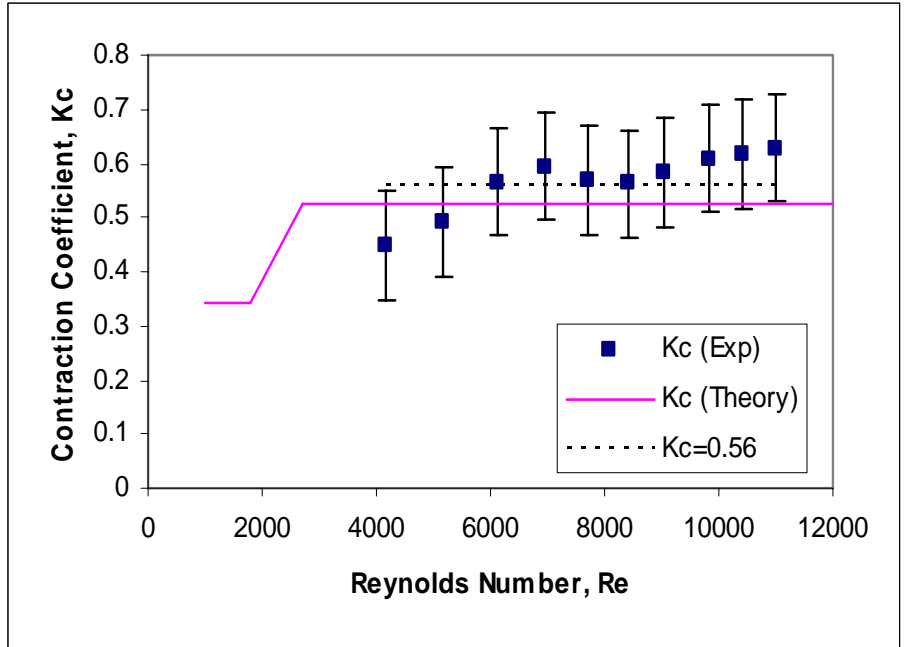


Figure 5.2 Loss coefficients for air-contraction

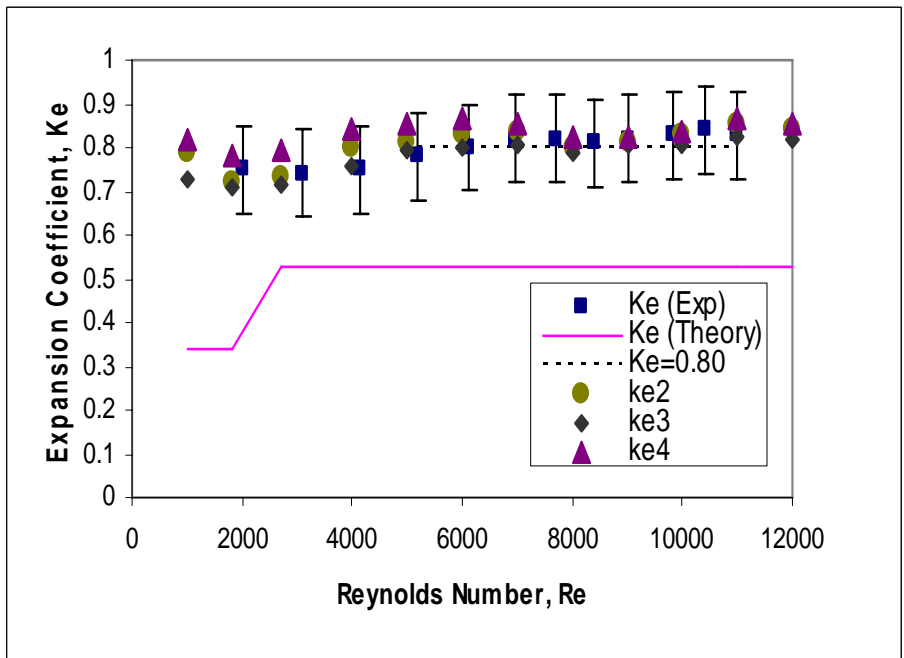


Figure 5.3 Repeatability in measuring the expansion loss coefficient

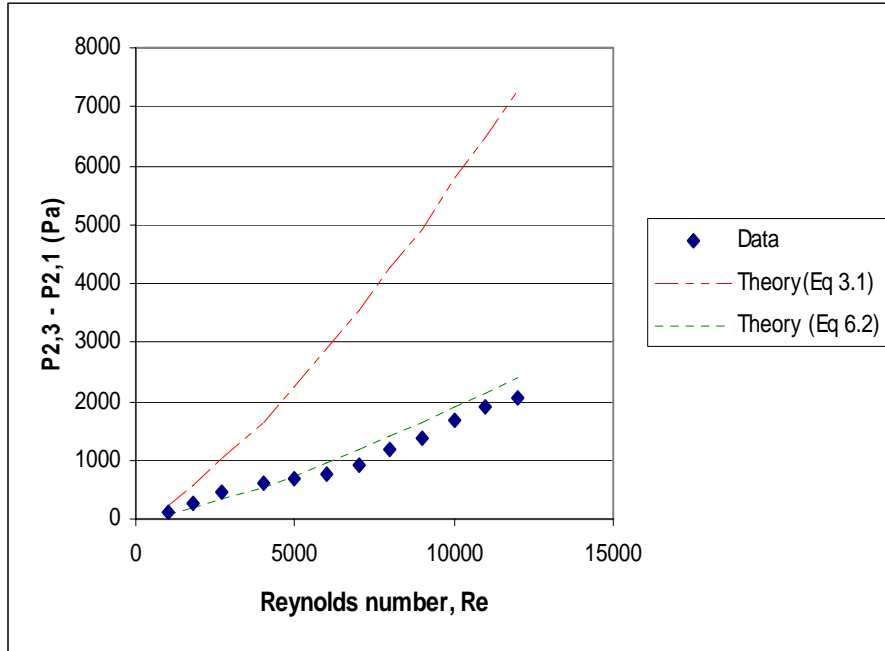


Figure 5.4 Comparison of the pressure data with theory for air-expansion

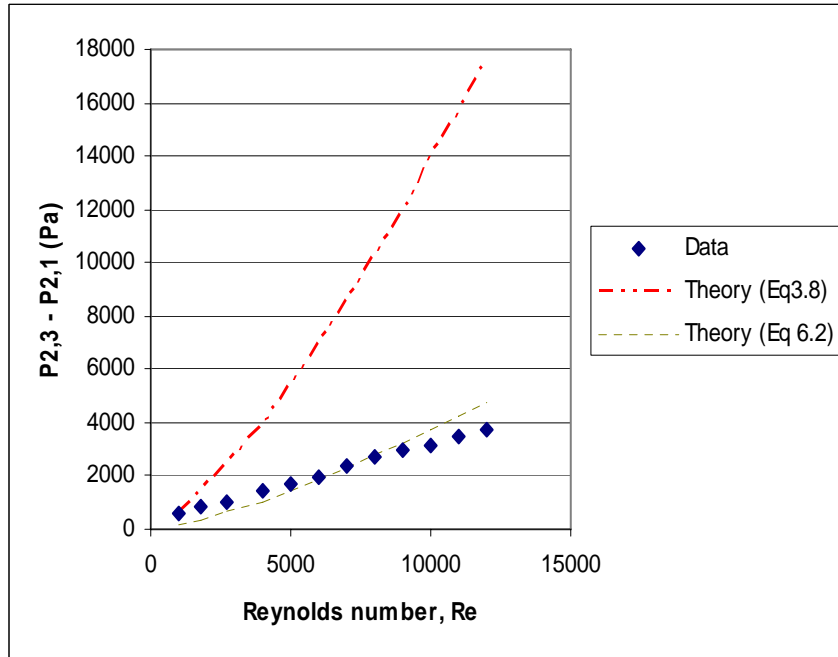


Figure 5.5 Comparison of the pressure data with theory for air-contraction

5.1.2 Single-Phase Flow with Liquid

The experimental data obtained for liquid water are summarized in Tables 5.3 for sudden expansion and in Table 5.4 for sudden contraction. This data are particularly interesting since they are virtually all in laminar flow, regime.

Figure 5.6 compares the experimental loss coefficients with the predictions of the Borda-Carnot relation, i.e., $K_e = (1 - \sigma)^2$. The experimental values of K_e are based on the assumption of flat velocity profiles, namely $k_{d1} = k_{d3} = 1$, and as noted, here the data correlate with $K_e = 0.75$ when $Re_{D3} \geq 400$. For lower Re_D values, however, K_e depends on Re_D , and the following correlation approximately applies:

$$K_e = a + b Re_D + c Re_D^2 \quad (5.3)$$

with, $a = -0.2154$, $b = 0.0043$ and $c = -5.10^{-6}$

Figure 5.7 compares the total measured pressure changes across the sudden expansion with Equation (3.1), this time $k_{d1} = k_{d3} = 1.3$ has been assumed. As expected, Equation (3.1) over predicts the total pressure change, wherever it is based on a loss coefficient that is smaller than the experimental value. It also overpredicts the total pressure change when the theoretical K_e (i.e., Equation (3.4)) is larger than what experiment suggests. However, with $k_{d1} = k_{d3} = 1$, when $K_e = 0.75$ for $Re_D \geq 400$ is used, and when Equation (6.3) is applied for $Re_D < 400$, the predicted and measured total pressure changes agree well.

Figure 5.8 compares the sudden contraction data for water with the prediction of the expression $K_c = (1 - 1/C_c)^2$, with C_c found from Equation (3.10). As can be noticed, the experimental data agree reasonably well with $K_c = 0.39$, while theory predicts a slightly lower value of $K_c = 0.38$. The experimental K_c values are evidently smaller than the values found for air ($K_c = 0.70$). This is understandable, however, since the data for air were virtually all associated with turbulent regime in the smaller channel, while for water

we deal with laminar flow. We thus deal with different ranges of Re_D in the two sets of experiments.

The experimental total pressure changes are compared with the predictions of Equation (3.8) in Figure 5.9, where now $k_{d1} = 1.3$ and $\beta_3 = 2$ are used. As noted, the data and theory (with $K_c = 0.38$) are in good agreement when flat velocity profiles are assumed everywhere, and using $K_c = 0.39$ only slightly improves the agreement between the data and the theoretical predictions.

5.1.3 Correlation of the Data

A comparison between Figures 5.1 and 5.6, where the loss coefficients for sudden expansion are shown, indicates that the air and water data are actually consistent. The two sets of data are shown together in Figure 5.10. As noted, over the range of $400 \leq Re_{D3} \leq 11,000$, a value of $Ke \approx 0.8$ along with assumed flat inlet and exit velocity profiles agrees with the experimental data very well. For lower Re_{D3} values, however, the above correlation (Equation 5.3) must be used.

The experimental data of Abdellal et al [3] for pressure loss in sudden expansion also are shown in Figure 5.10. The reported loss coefficients by Abdellal are consistently lower than the values obtained in this study. While the reason for this disagreement is not known for sure, two issues can be pointed out. First, the data of Abdellal have relatively large uncertainty or error bands. Second, the possibility of a systematic error in the experiments that were analyzed by Abdellal can be hardly rejected.

Also shown in Figure 5.10 are the loss coefficients that were extracted from a table in the hydraulics handbook authored by King (1996). The depicted curve only covers the range of parameters that were directly represented in the aforementioned table. As noted, the loss coefficients obtained from King (1996) are not in good agreement with our data, and indicate that the loss coefficients in the present experiments were significantly higher than what is expected in conventional macro systems.

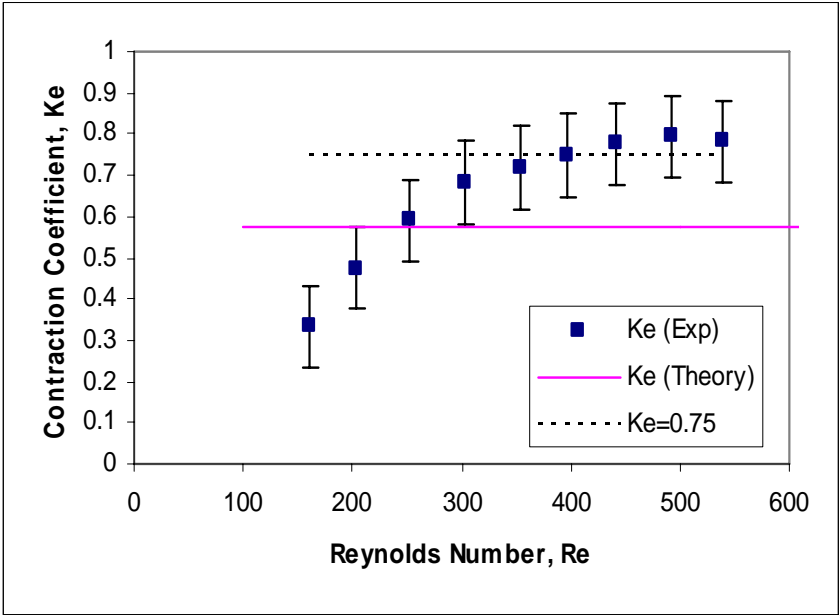


Figure 5.6 Loss coefficients for water-expansion

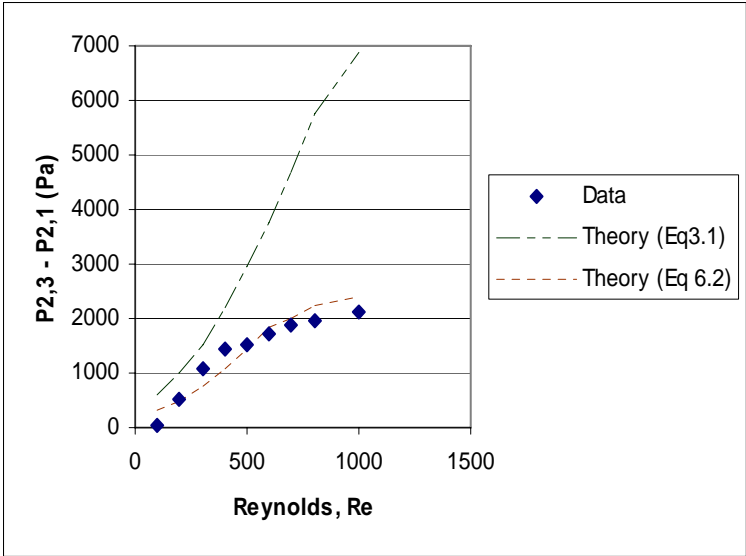


Figure 5.7 Comparison of the pressure data with theory for water-expansion

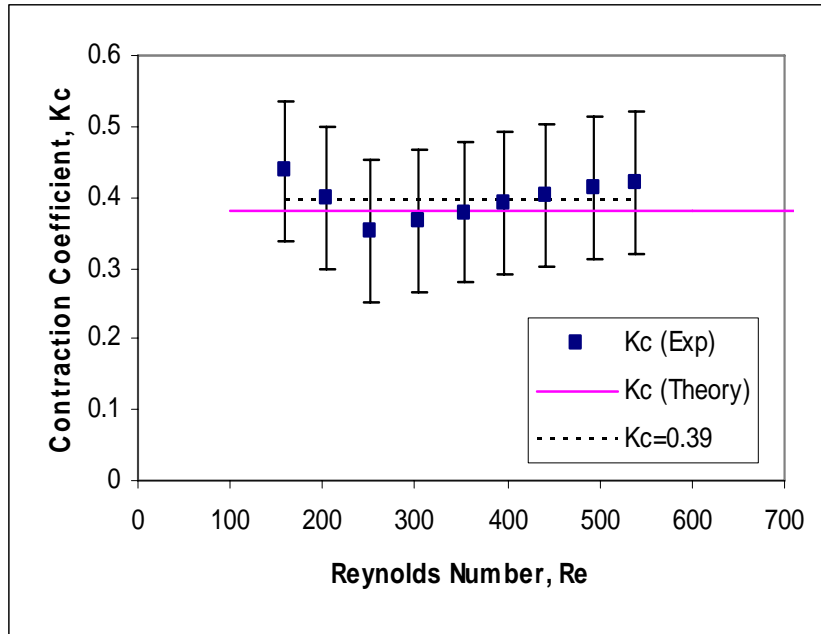


Figure 5.8 Loss coefficients for water-contraction

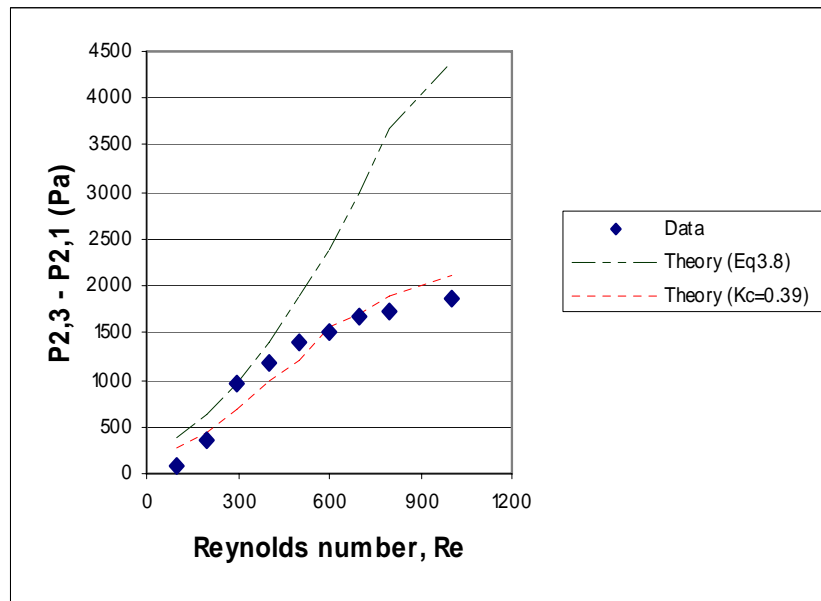


Figure 5.9 Comparison of the pressure data with theory for water-contraction

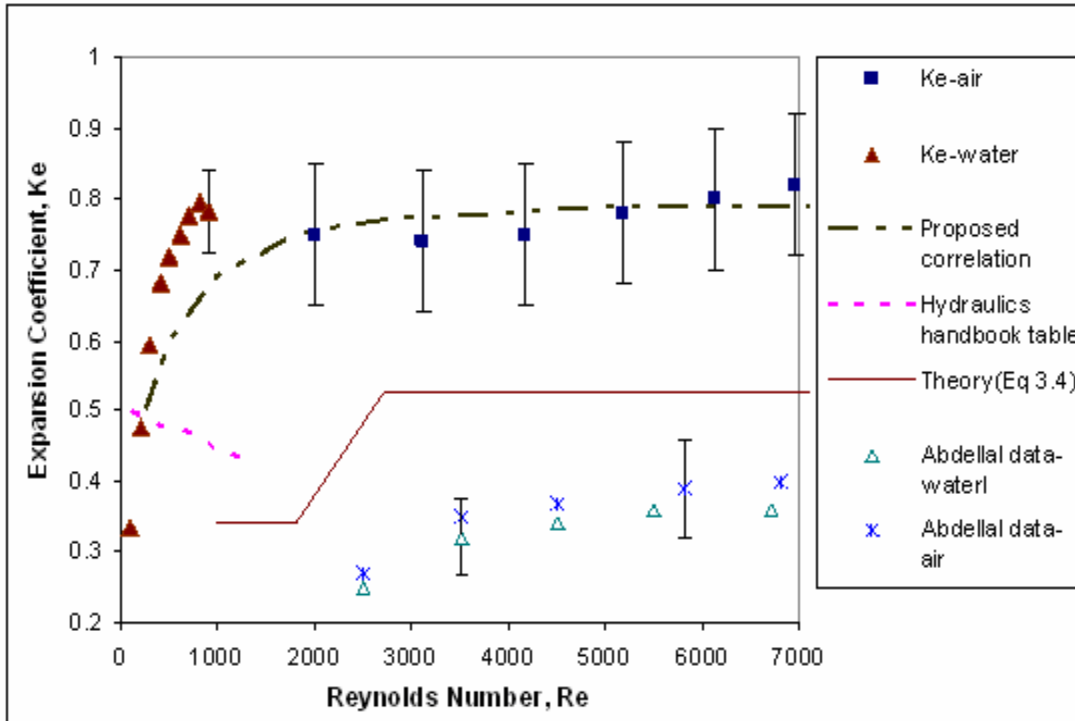


Figure 5.10 Loss coefficient data for air and water expansion

Figure 5.11 depicts all the single-phase sudden contraction data in this investigation, where K_c has been obtained based on flat velocity profiles at both inlet and outlet. Unlike the sudden expansion case, a constant value can not be assumed everywhere. The data, however, suggest the following possible correlation;

$$K_c = 0.0588 \ln(Re) + 0.0218 \quad (5.4)$$

As noted, the above correlation agrees with data very well, except at very low Re_{D3} values ($Re_{D3} \leq 200$), where the data indicate $K_c \approx 0.4$.

The experimental data of Abdellal are shown in the figure. The single-phase flow experimental data points of Abdellal et al [3] are few, and have relatively large error bands. Nevertheless, for Reynolds numbers larger than 4,000 they are in reasonable agreement with the data presented in this study. The loss coefficients obtained by interpolation in a table in King (1996) are also shown in the figure. The latter table,

needless to say, is applicable to conventional systems. The depicted curve only covers the range of parameters that were directly represented in the aforementioned table. As noted, the loss coefficients obtained from King (1996) are not in good agreement with our data, and indicate that the loss coefficient in the present experiments were significantly higher than what is expected in conventional macro-systems.

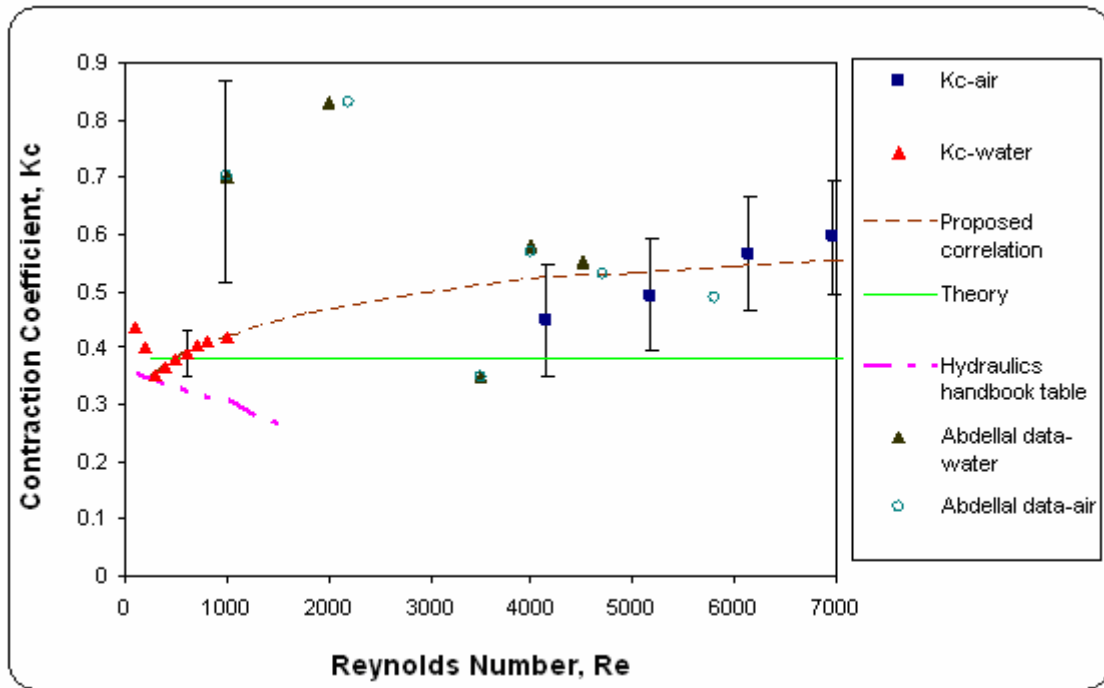


Figure 5.11 Loss coefficient data for air and water contraction

Table 5.3

Single-phase flow through sudden expansion- Experimental data for water

\dot{m} (g/s)	Re	$P_{2,3}-P_{2,1}$ (kPa)	$K_c(\text{exp})$	$K_c(\text{th})$
0.1033	160	0.577	0.33	0.52
0.1315	204	1.031	0.47	0.52
0.1626	252	1.271	0.59	0.52
0.1956	303	1.441	0.68	0.52
0.2273	353	1.516	0.71	0.52
0.2561	397	1.736	0.74	0.52
0.2865	442	1.874	0.77	0.52
0.3175	493	1.979	0.79	0.52
0.3476	539	2.127	0.78	0.52

Table 5.4

Single-phase flow through sudden contraction- Experimental data for water

\dot{m} (g/s)	Re	$P_{2,3}-P_{2,1}$ (kPa)	$K_c(\text{exp})$	$K_c(\text{th})$
0.1033	160	0.087	0.43	0.38
0.1315	204	0.351	0.40	0.38
0.1626	252	0.953	0.35	0.38
0.1956	303	1.190	0.37	0.38
0.2273	353	1.403	0.38	0.38
0.2561	397	1.515	0.39	0.38
0.2865	442	1.682	0.40	0.38
0.3175	493	1.733	0.41	0.38
0.3476	539	1.978	0.42	0.38

5.2 Two-Phase flow, Flow Area Expansion

The experimental data obtained for two-phase flow for flow area expansion are summarized in Table 5.5.

Figures 5.12, 5.13, 5.14 and 5.15 compare the experimental values of the total pressure drop across the sudden flow area expansion with the prediction of Equations (3.12) and (3.13). The latter equation of course needs a void-quality or slip ratio relation. Thus, in Figures 5.12 through 5.15, theoretical results are shown for three flow models: homogeneous flow; slip flow based on Zivi's correlation [35] where $S = (\rho_L / \rho_G)^{1/3}$; and the slip flow correlation of Premoli et al [36]. The correlation of Premoli et al [36] is:

$$S = 1 + E_1 \left(\frac{y}{1 + yE_2} - yE_2 \right)^{1/2} \quad (5.5)$$

where

$$y = \frac{\beta}{1 - \beta} \quad (5.6)$$

$$\beta = \frac{\langle J_G \rangle}{\langle J \rangle} \quad (5.7)$$

$$E_1 = 1.578 \text{Re}_{LO}^{-0.19} \left(\frac{\rho_L}{\rho_G} \right)^{0.22} \quad (5.8)$$

$$E_2 = 0.0273 \text{We} \text{Re}_{LO}^{-0.51} \left(\frac{\rho_L}{\rho_G} \right)^{-0.08} \quad (5.9)$$

$$We = \frac{G^2 D_H}{\sigma \rho_L} \quad (5.10)$$

$$Re_{LO} = \frac{GD_H}{\mu_L} \quad (5.11)$$

In the above equations β is the volumetric quality.

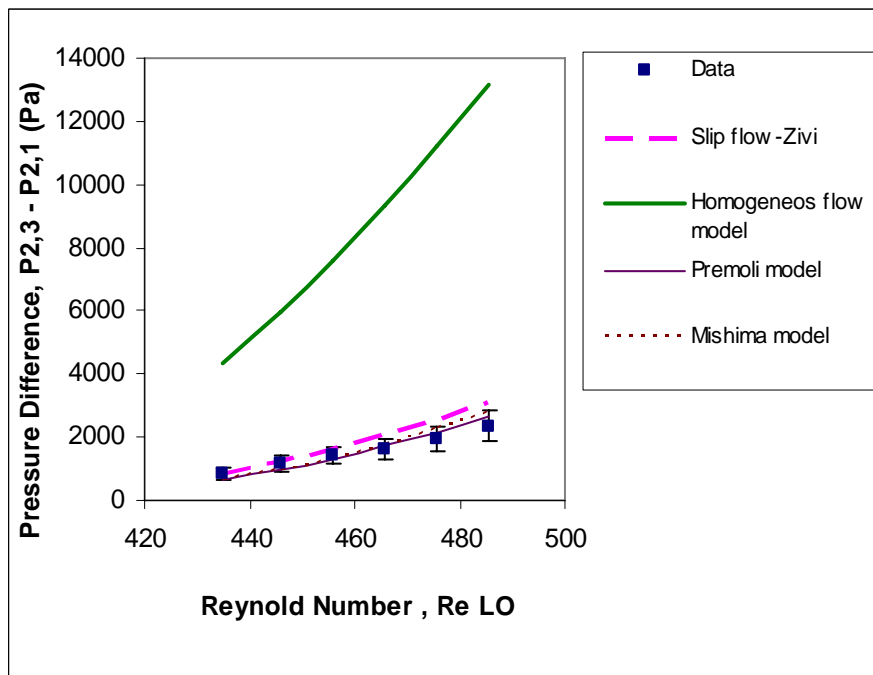


Figure 5.12 Two-phase expansion pressure drop for
 $\dot{m}_L = 0.2560$ g/s, $\dot{m}_G = 0.0243$ to 0.0568 g/s.

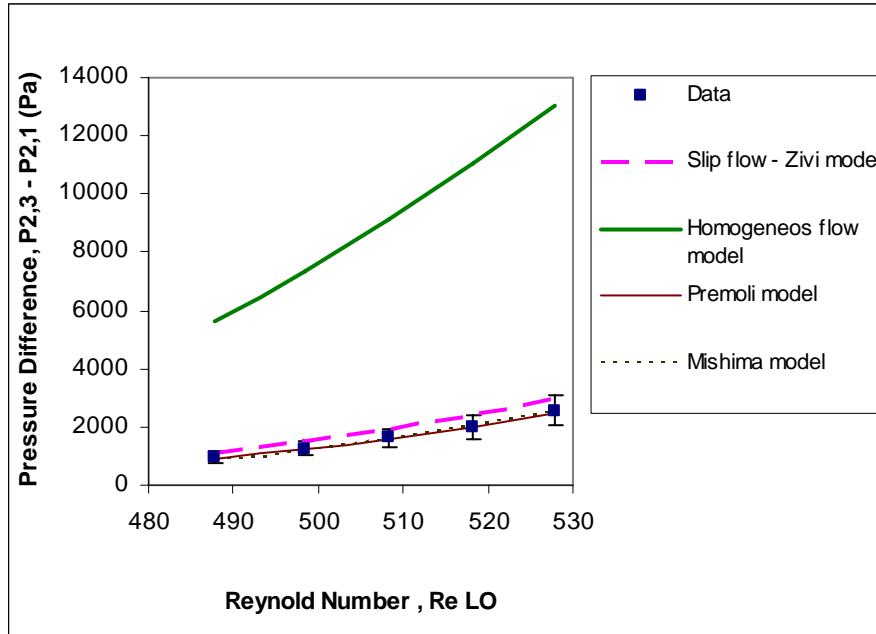


Figure 5.13 Two-phase expansion pressure drop for

$$\dot{m}_L = 0.2865 \text{ g/s}, \dot{m}_G = 0.0278 \text{ to } 0.0536 \text{ g/s.}$$

As noted, all four figures indicate that the homogeneous model performs very poorly, and results in very significant over prediction of the total pressure drop for all cases. The over prediction can in fact be by as much as an order of magnitude. The data thus suggest the occurrence of very significant velocity slip.

Figures 5.12 and 5.13 indicate that the slip flow models of Zivi [35] and Premoli et al [36] both predict the depicted data very well. These data were obtained at relatively low liquid flow rates. For the data in Figure 5.12 we have

$$J_L = 0.46 \text{ m/s} \quad ; J_G = 9.68 - 15.56 \text{ m/s}$$

$$Re_L = 434.9 - 485.4$$

For the data in Figure 5.13 we have

$$J_L = 0.51 \text{ m/s} \quad ; J_G = 10.15 - 16.09 \text{ m/s}$$

$$Re_L = 487.7 - 527.8$$

The close agreement between data and the two slip correlations suggest that the flow regime has been predominantly annular in these data.

Figures 5.14 and 5.15 represent conditions where the flow regime was probably intermittent (bubbly, slug, plug). For Figure 5.14, we have

$$J_L = 0.57 \text{ m/s} \quad ; J_G = 7.09 - 14.9 \text{ m/s}$$
$$Re_L = 519.1 - 570.9$$

For Figure 5.15, furthermore, we have

$$J_L = 0.57 \text{ m/s} \quad ; J_G = 3.83 - 9.27 \text{ m/s}$$
$$Re_L = 506.9 - 533.1$$

As can be seen in Figures 5.14 and 5.15, the slip ratio expression of Zivi [35] and Premoli et al [36] lead to substantial underprediction of the total pressure drop, typically by a factor of 2. The homogeneous flow, on the other hand, overpredicts the data by a large margin.

The above data suggest that the two-phase pressure drop across a miniature sudden expansion is flow regime-dependent. This is of course to be expected.

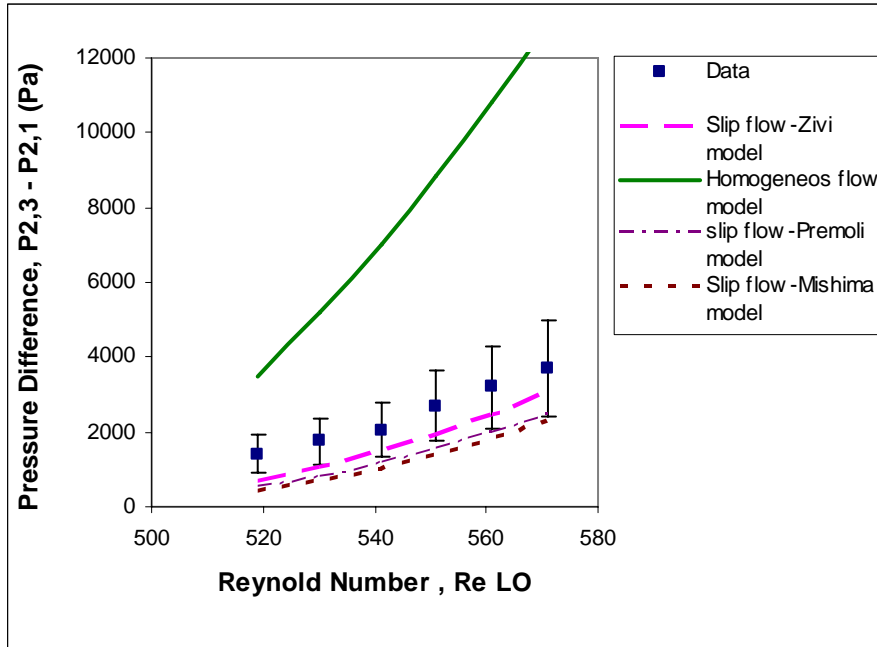


Figure 5.14 Two-phase expansion pressure drop for
 $\dot{m}_L = 0.3174 \text{ g/s}$, $\dot{m}_G = 0.0171 \text{ to } 0.0505 \text{ g/s}$.

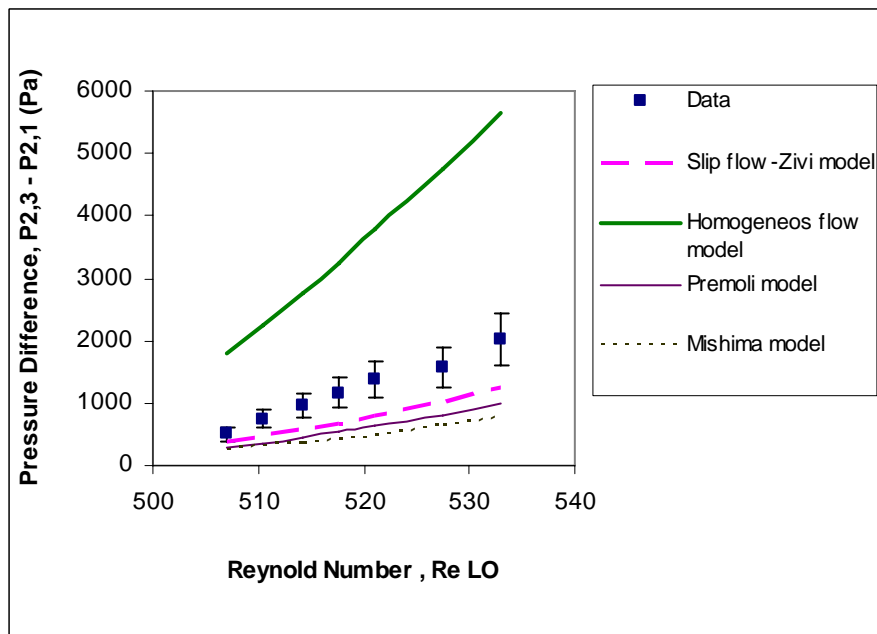


Figure 5.15 Two-phase expansion pressure drop for
 $\dot{m}_L = 0.3174 \text{ g/s}$, $\dot{m}_G = 0.0093 \text{ to } 0.0261 \text{ g/s}$.

On Figures 5.14 and 5.15, the predictions of Equations (3.12) and (3.13) are also shown when the following drift flux correlation of Mishima and Hibiki [37] is used as a substitute for the slip ratio:

$$\alpha = \frac{j_G}{C_0 j + V_{gi}} \quad (5.12)$$

with;

$$V_{gi} \approx 0$$

$$C_0 = 1.2 + 0.51 \exp(-0.692D)$$

where D is in mm.

The results obtained with the above drift flux model, as noted, are similar to the other two slip ratio correlations.

As a rough empirical fix, the predictions of a slip flow model are also shown in Figures 5.16, 5.17, 5.18 and 5.19, where the slip ratio is assumed to be

$$S = c \left(\frac{\rho_L}{\rho_G} \right)^{1/3} \quad (5.13)$$

where c is a constant to be found experimentally. As noted, good agreement is obtained between data and the correlation with c = 0.7.

Alternatively, the correlation of Armand [38] can be used:

$$\alpha = C_A \beta \quad (5.14)$$

where $\beta = j_G / j$ is the volumetric quality. The predictions of Equations (3.12) and (3.14), along with Equation (3.11) are shown in Figures 5.16 through 5.19. As noticed, the predictions agree with the experimental data with $C_A = 0.5$.

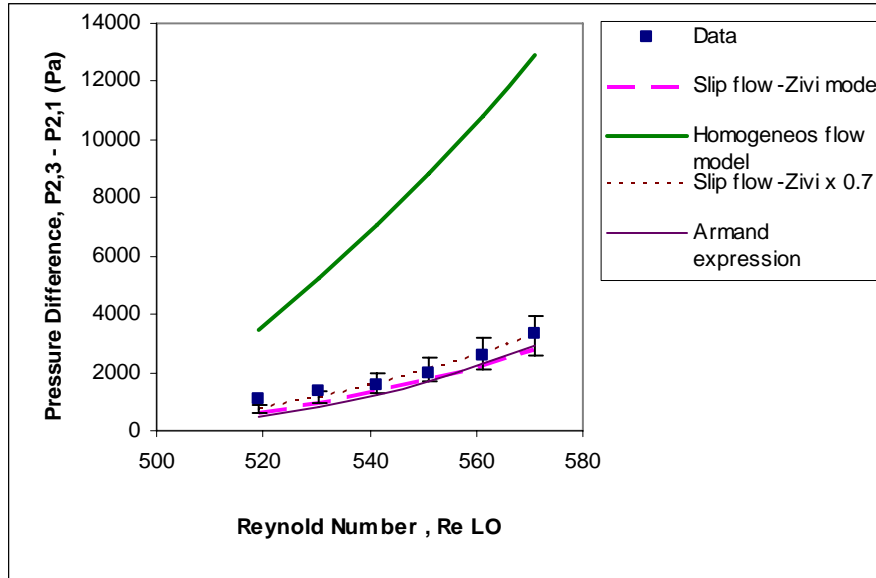


Figure 5.16 Two-phase expansion pressure drop for

$$\dot{m}_L = 0.2560 \text{ g/s}, \dot{m}_G = 0.0243 \text{ to } 0.0568 \text{ g/s.}$$

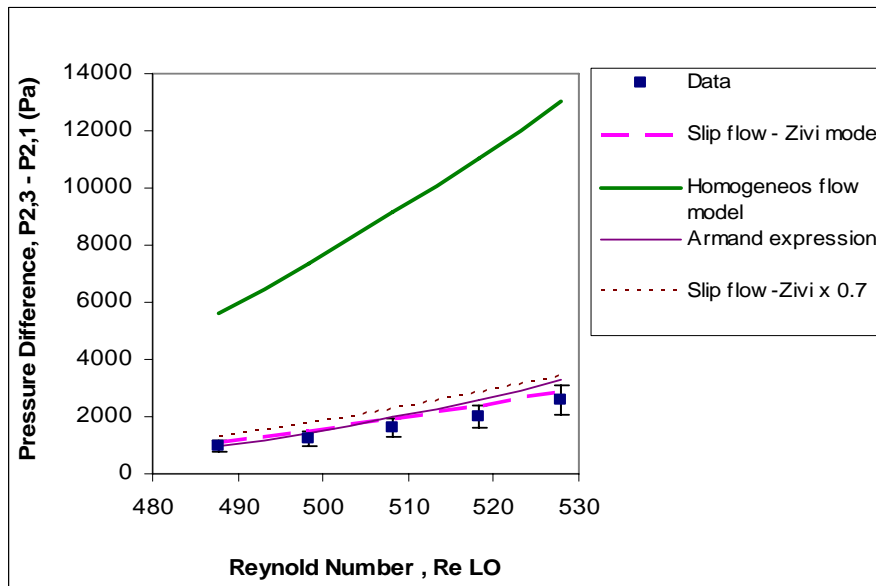


Figure 5.17 Two-phase expansion pressure drop for

$$\dot{m}_L = 0.2865 \text{ g/s}, \dot{m}_G = 0.0278 \text{ to } 0.0536 \text{ g/s.}$$

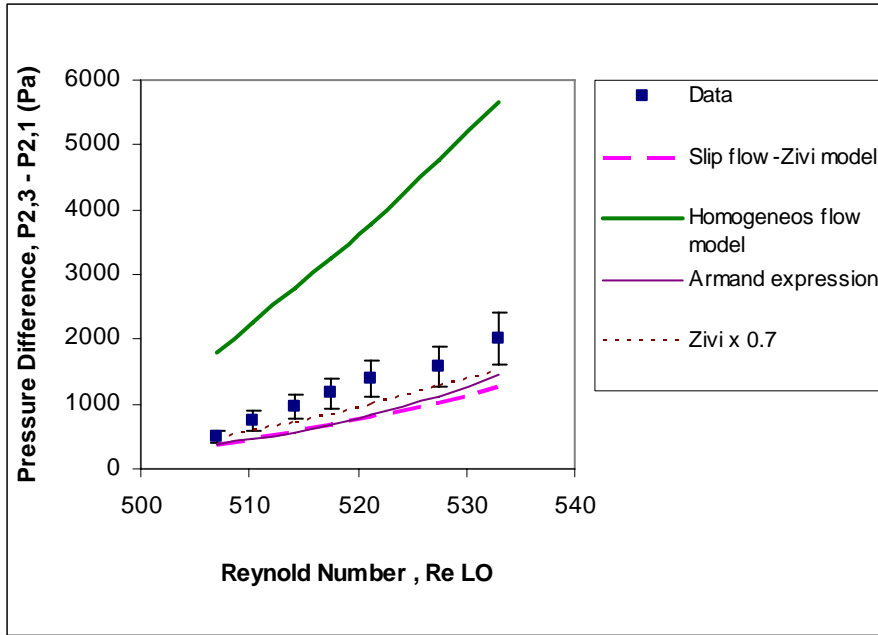


Figure 5.18 Two-phase expansion pressure drop for
 $\dot{m}_L = 0.3174 \text{ g/s}$, $\dot{m}_G = 0.0171 \text{ to } 0.0505 \text{ g/s}$.

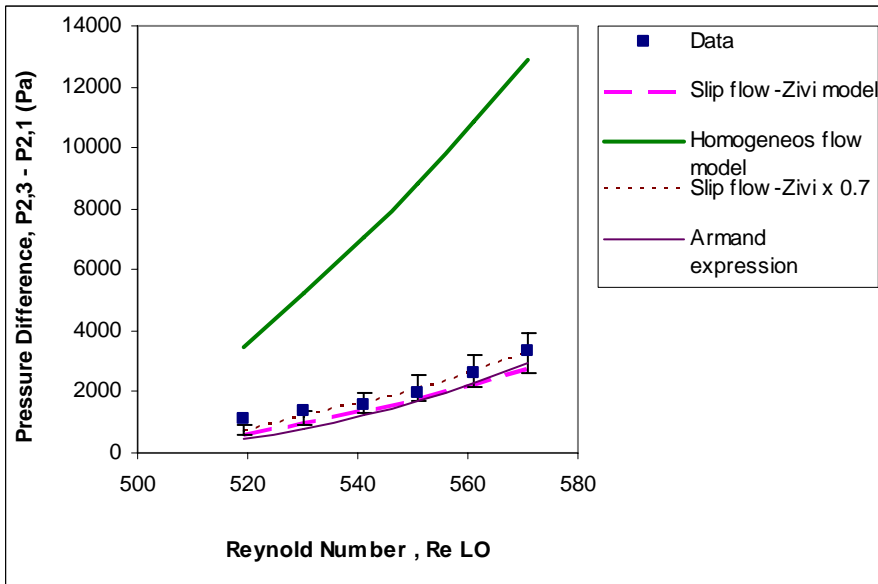


Figure 5.19 Two-phase expansion pressure drop for
 $\dot{m}_L = 0.3174 \text{ g/s}$, $\dot{m}_G = 0.0093 \text{ to } 0.0261 \text{ g/s}$

Table 5.5

Two-phase flow through sudden expansion- Experimental data

\dot{m}_L (g/s)	\dot{m}_G (g/s)	$Re_{L0,1}$	$P_{2,3}-P_{2,1}$ (Pa)	ΔP_h (Pa)	ΔP_s (Pa)
0.2560	0.0243	434.9	940	4372.26	1102.29
0.2560	0.0313	445.8	1468	5974.51	1567.88
0.2560	0.0377	455.8	1824	7578.41	2056.33
0.2560	0.0442	465.8	2220	9343.25	2613.78
0.2560	0.0505	475.6	2540	11184.47	3213.11
0.2560	0.0568	485.4	2850	13154.34	3870.53
0.2865	0.0278	487.7	1083	5624.01	1422.42
0.2865	0.0346	498.3	1646	7367.86	1929.46
0.2865	0.0410	508.2	2013	9146.04	2468.52
0.2865	0.0474	518.2	2502	11056.97	3067.53
0.2865	0.0536	527.8	3066	13034.79	3704.99
0.3174	0.0093	506.9	801	1806.18	640.04
0.3174	0.0115	510.4	1051	2258.91	795.91
0.3174	0.0139	514.1	1261	2770.69	978.07
0.3174	0.0161	517.5	1465	3256.22	1156.16
0.3174	0.0184	521.1	1680	3780.59	1353.71
0.3174	0.0225	527.4	1970	4757.86	1734.67
0.3174	0.0261	533.1	2520	5660.87	2099.61
0.3174	0.0171	519.1	1416	3482.10	827.08
0.3174	0.0243	530.3	1756	5204.11	1275.72
0.3174	0.0313	541.1	2062	7039.38	1784.65
0.3174	0.0377	551.1	2685	8856.32	2312.73
0.3174	0.0442	561.2	3188	10837.53	2910.43
0.3174	0.0505	570.9	3705	12888.47	3548.77

5.3 Two-Phase flow, Flow Area Contraction

The experimental data obtained for two-phase flow through flow area contraction are summarized in Table 5.6. In Figures 5.20 through 5.23 the total experimental values of the total pressure changes across the sudden contraction (i.e., $P_{2,3} - P_{2,1}$ in Figure 3.1) are compared with the predictions of Equation (3.21). The calculated pressure changes in these figures are all based on the assumption that vena-contracta occurs, and that the contraction coefficient C_c is found from the correlation of Geiger [26] (Equation (3.10)).

For the data in Figure 5.20 we have

$$J_L = 0.64 \text{ m/s} \quad ; J_G = 2.83 - 8.54 \text{ m/s}$$
$$Re_L = 559.6 - 586.9$$

For Figure 5.21 we have

$$J_L = 1.13 \text{ m/s} \quad ; J_G = 2.83 - 10.16 \text{ m/s}$$
$$Re_L = 986.4 - 1018.9$$

For Figure 5.22 we have

$$J_L = 0.46 \text{ m/s} \quad ; J_G = 3.87 - 12.20 \text{ m/s}$$
$$Re_L = 411.8 - 442.9$$

For Figure 5.23 we have

$$J_L = 0.51 \text{ m/s} \quad ; J_G = 2.83 - 10.16 \text{ m/s}$$
$$Re_L = 455.2 - 482.5$$

Table 5.6

Two-phase flow through sudden contraction- Experimental data

\dot{m}_L (g/s)	\dot{m}_G (g/s)	$Re_{L0,1}$	$P_{2,3}-P_{2,1}$ (Pa)	ΔP_h (Pa)	ΔP_s (Pa)
0.2561	0.0093	411.8	491	4237.69	1084.55
0.2561	0.0139	419.0	755	6375.07	1829.35
0.2561	0.0183	425.8	1031	8485.33	2721.34
0.2561	0.0225	432.3	1260	10559.70	3736.11
0.2561	0.0261	437.9	1711	12384.39	4732.76
0.2561	0.0293	442.9	2063	14042.49	5716.91
0.2865	0.0068	455.2	644	3474.53	848.92
0.2865	0.0093	459.0	857	4730.08	1188.83
0.2865	0.0115	462.5	1154	5852.10	1535.64
0.2865	0.0161	469.6	1371	8249.99	2403.28
0.2865	0.0205	476.4	1805	10609.29	3412.66
0.2865	0.0244	482.5	2556	12754.14	4453.71
0.3538	0.0068	559.6	601	4320.37	1061.68
0.3538	0.0093	563.5	1054	5855.17	1436.95
0.3538	0.0115	566.9	1665	7222.94	1815.75
0.3538	0.0161	574.0	1780	10134.67	2751.44
0.3538	0.0205	580.8	1970	12985.46	3826.59
0.3538	0.0244	586.9	2220	15565.95	4926.20
0.6288	0.0068	986.4	1056	7965.01	2201.95
0.6288	0.0093	990.2	1316	10640.92	2709.05
0.6288	0.0115	993.7	1356	13012.86	3211.56
0.6288	0.0161	1000.8	1462	18024.21	4416.40
0.6288	0.0205	1007.6	1885	22883.33	5755.34
0.6288	0.0244	1013.7	2488	27243.94	7091.28
0.6288	0.0278	1018.9	3205	31086.65	8369.34

All the aforementioned depicted cases clearly show that the homogeneous flow assumption overpredicts the total pressure drop very significantly; this result is consistent with the data representing sudden expansion. They thus confirm the occurrence of significant velocity slip between the two-phases. The displayed results also show that the slip flow models of Zivi (1964) and Premoli et al (1972), as well as the drift flux model of Mishima and Hibiki (1996) all improve the accuracy of the calculations. Neither of the slip flow correlations leads to a generally good agreement between the data and predictions, however. The discrepancy between the data and predictions in fact increases monotonically with increasing Re_{LO} for all the depicted cases.

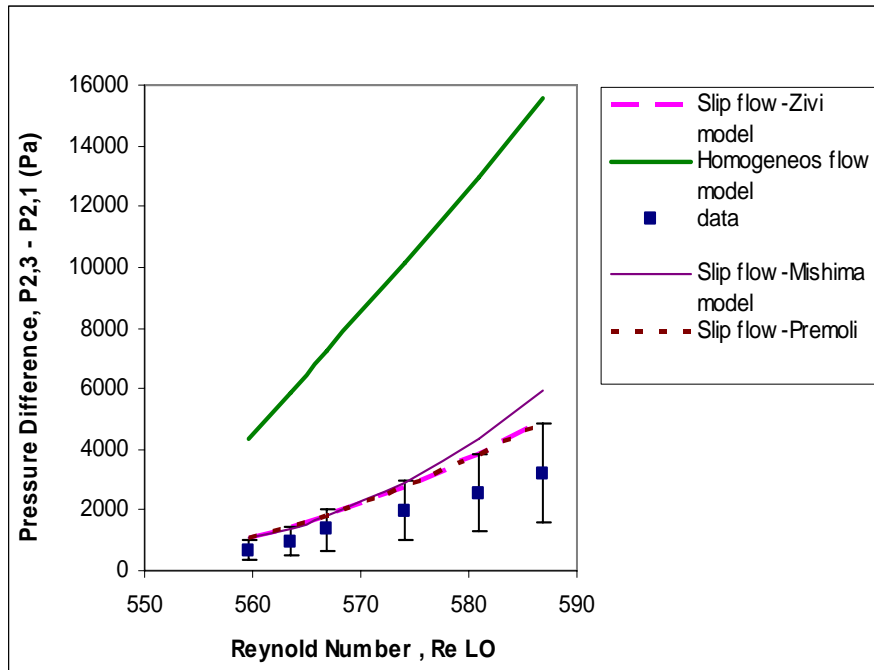


Figure 5.20 Two-phase contraction pressure drop for

$\dot{m}_L = 0.3538$ g/s, $\dot{m}_G = 0.0068$ to 0.0244 g/s; model predictions assume the occurrence of vena-contracta.

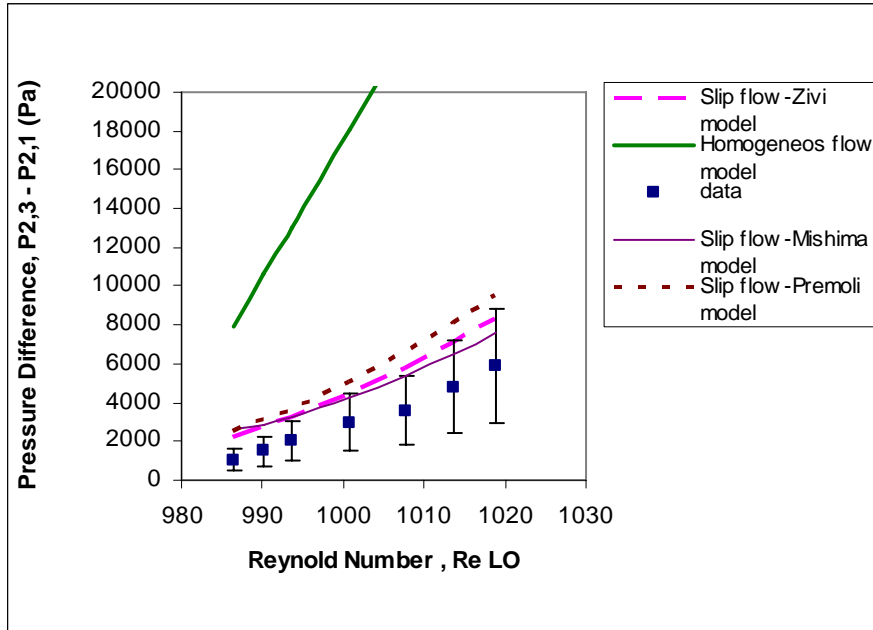


Figure 5.21 Two-phase contraction pressure drop for

$\dot{m}_L = 0.6288 \text{ g/s}$, $\dot{m}_G = 0.0068 \text{ to } 0.0278 \text{ g/s}$; model predictions assume the occurrence of vena-contracta.

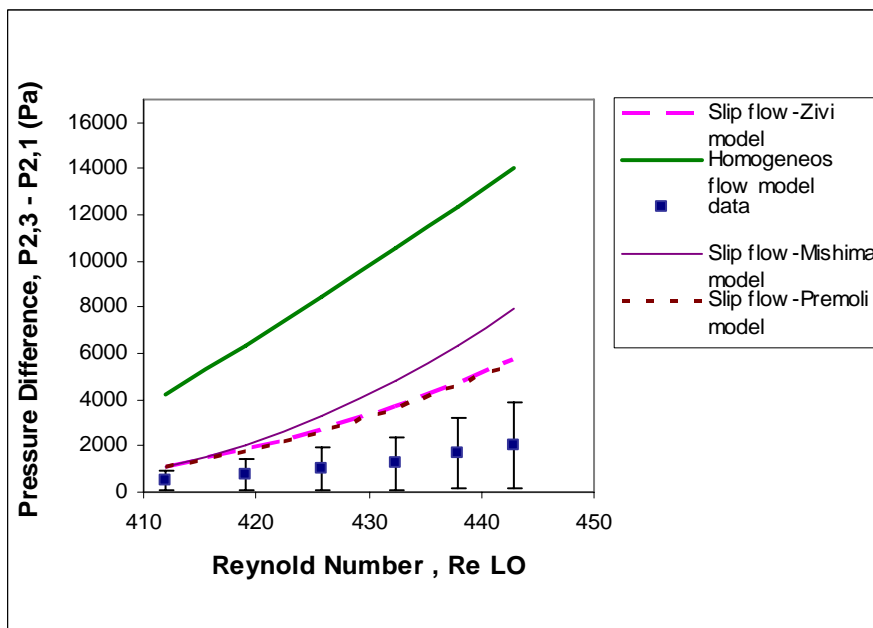


Figure 5.22 Two-phase contraction pressure drop for

$\dot{m}_L = 0.2561 \text{ g/s}$, $\dot{m}_G = 0.0093 \text{ to } 0.0293 \text{ g/s}$; model predictions assume the occurrence of vena-contracta.

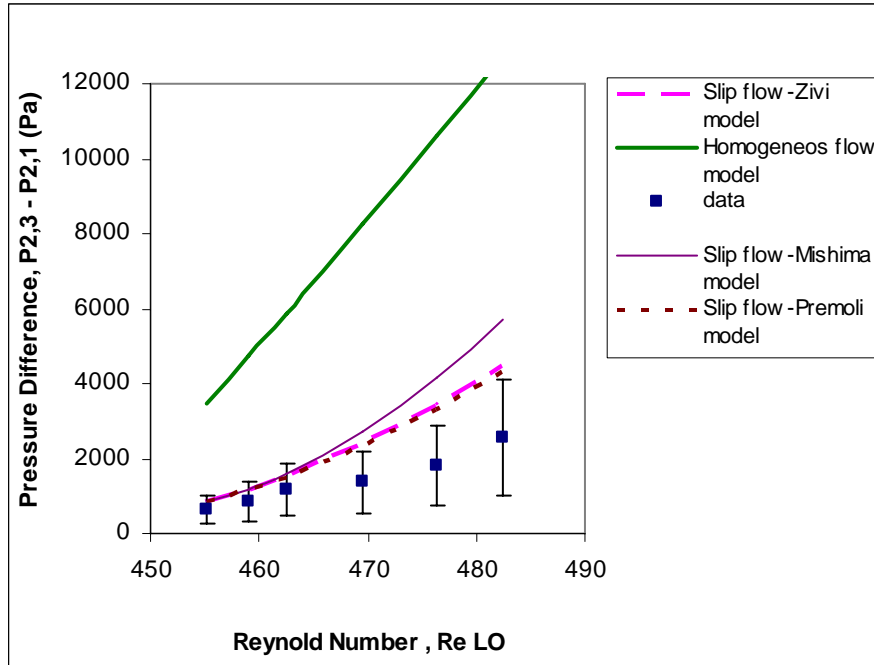


Figure 5.23 Two-phase contraction pressure drop for

$\dot{m}_L = 0.2865 \text{ g/s}$, $\dot{m}_G = 0.0068 \text{ to } 0.0244 \text{ g/s}$; model predictions assume the occurrence of vena-contracta.

Figures 5.24, 5.25, 5.26 and 5.27 display the results for two-phase pressure drop in the sudden contraction experiments, when no vena-contracta is assumed (i.e., when $C_c = 1$ in Equation 3.8, where $k_{d1} = \beta_3 = 1$ are assumed). The predictions designated as slip flow model in fact represent the slip ratio expression of Zivi [35], without any adjustment. The predictions of the slip flow model are in excellent agreement with the experimental data in Figures 5.25 through 5.27. For the lowest liquid mass flow rate, depicted in Figure 5.24, the prediction based on the Zivi slip ratio are higher than the experimental data, with the discrepancy approaching a factor of 2. The data indicate the occurrence of a slip ratio larger than the slip ratio of Zivi.

Based on the results depicted in Figures 5.24 through 5.27, it can thus be concluded that the assumption of no vena-contracta, along with the slip ratio correlation of Zivi [35]

will be appropriate for the calculation of the total pressure change across a sudden contraction in mini-channels. This observation may not be accurate at very low liquid superficial velocities, as noted in Figure 5.24. A correction in the slip ratio expression of Zivi may thus be needed for low liquid superficial velocity conditions. However, our experimental data is not sufficiently detailed for the development of such an empirical correlation at this point.

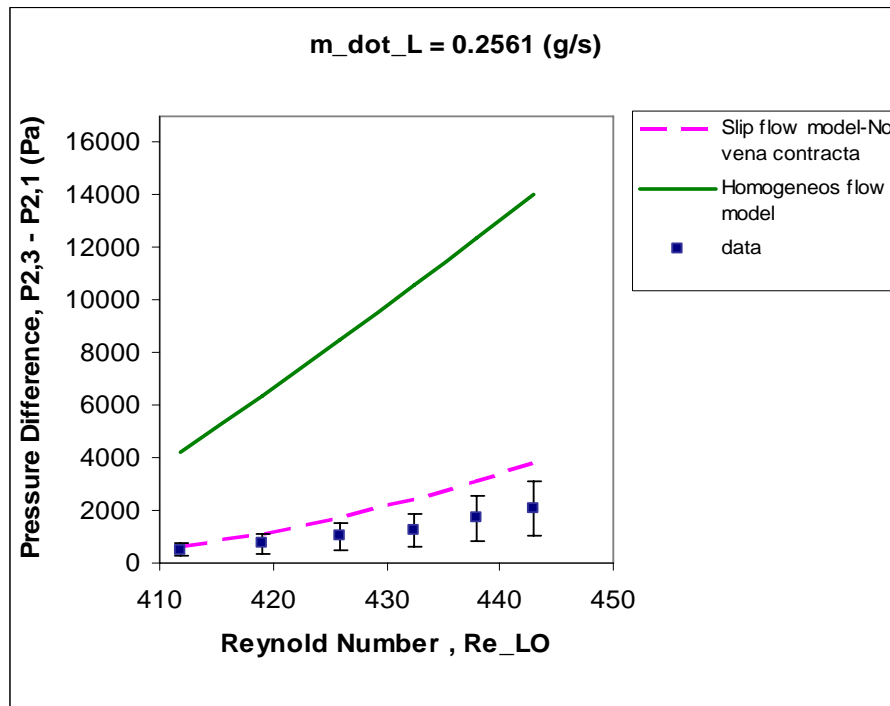


Figure 5.24 Two-phase contraction pressure change with no vena-contracta for

$$\dot{m}_L = 0.2561 \text{ g/s}, \dot{m}_G = 0.0093 \text{ to } 0.0293 \text{ g/s};$$

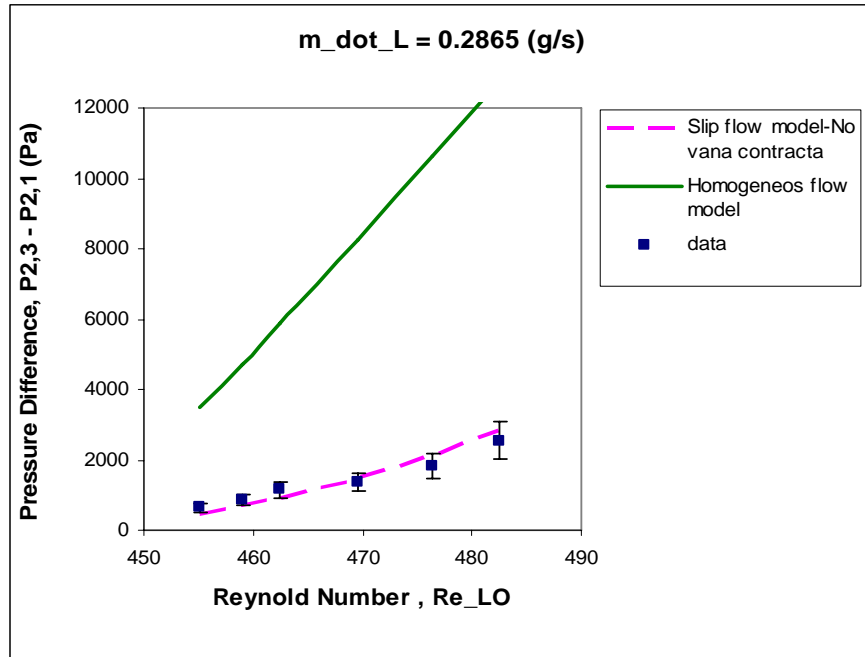


Figure 5.25 Two-phase contraction pressure change with no vena-contracta for $\dot{m}_L = 0.2865 \text{ g/s}$, $\dot{m}_G = 0.0068 \text{ to } 0.0244 \text{ g/s}$

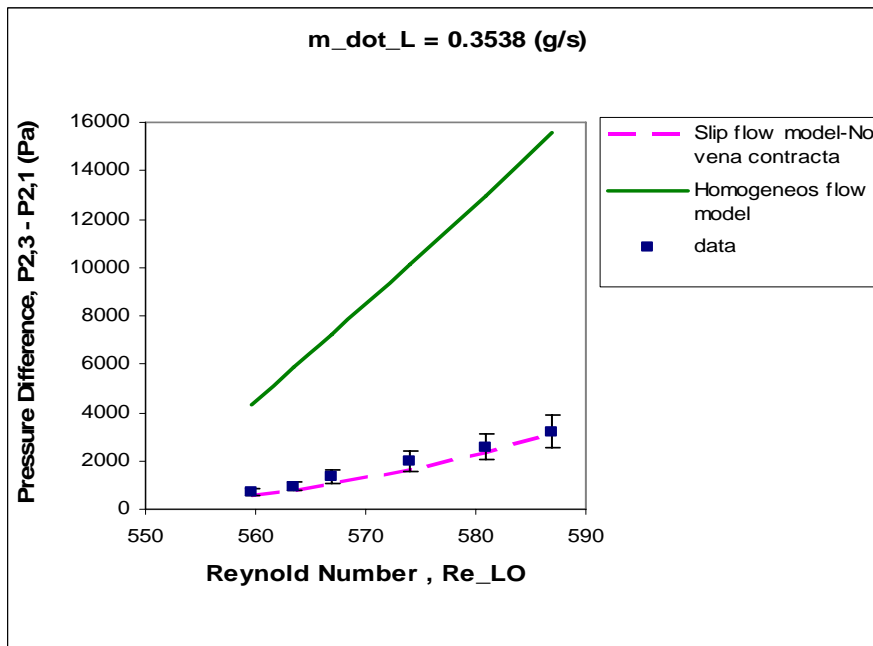


Figure 5.26 Two-phase contraction pressure change with no vena-contracta for $\dot{m}_L = 0.3538 \text{ g/s}$, $\dot{m}_G = 0.0068 \text{ to } 0.0244 \text{ g/s}$

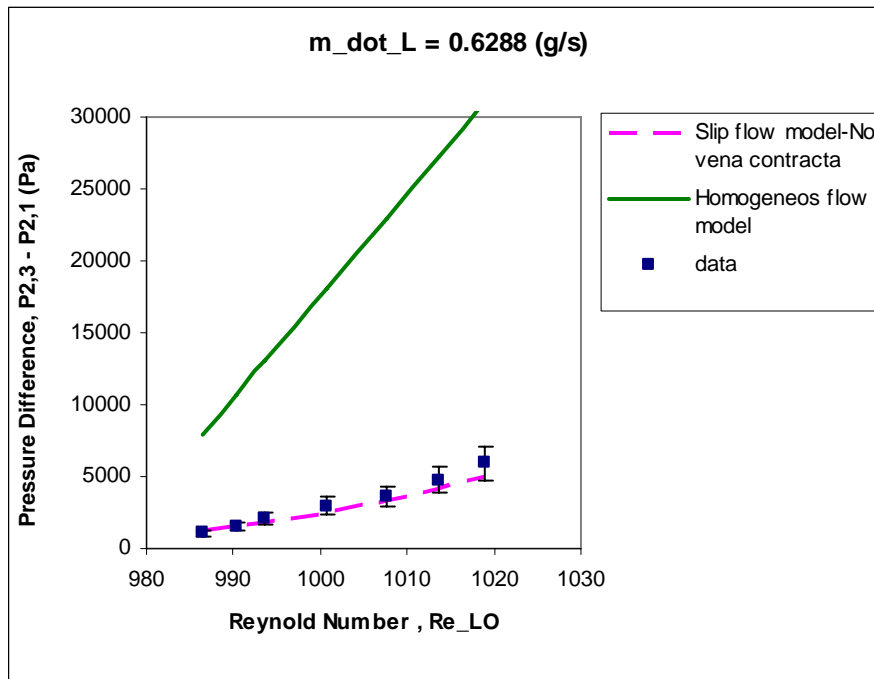


Figure 5.27 Two-phase contraction pressure change with no vena-contracta for

$$\dot{m}_L = 0.6288 \text{ g/s}, \dot{m}_G = 0.0068 \text{ to } 0.0278 \text{ g/s}$$

6 CONCLUDING REMARKS

6.1 Conclusion

In this investigation, the pressure drops associated with single-phase as well as two-phase flows through miniature flow area expansion and contraction were experimentally studied. The flow area change for both expansion and contraction represented the interface between two capillaries; one with a diameter of 0.84 mm, the other with a diameter of 1.6 mm. experiments were performed with single-phase air, single-phase water, and air-water two-phase mixtures with various flow qualities.

The results of the investigation lead to the following conclusions:

- 1 For single-phase flow through a sudden flow area expansion, the air and water data were consistent; although they represented different ranges of Re . The conventional theory did not predict the experimental data well. A simple correlation for the loss coefficient could be developed, however.
- 2 For single-phase flow through a sudden flow area contraction, the conventional theory that is based on the vena-contracta phenomenon in the smallest channel, agreed with the experimental data for $Re \geq 6,000$. For lower values of Re , however, the loss coefficient varied with Re . The experimental loss coefficients were correlated empirically for the entire range of the experimental data.
- 3 For two-phase pressure drop across the sudden expansion, the widely applied homogeneous flow assumption leads to a significant over prediction of the pressure change. The trends in the experimental data suggest a strong slip between the two phases. Good agreement between the data and one-dimensional flow theory was obtained with a simple correlation for the slip

ratio. The ratio was either found from a modified Zivi's expression, or from an Armand-type void fraction-quality expression.

- 4 For two-phase pressure drop across a sudden contraction, once again the one-dimensional homogeneous flow theory was found to be totally inadequate, and overpredicted the experimental data systematically, and very significantly. The one-dimensional slip flow model without the vena-contracta phenomenon, however, agreed well with the experimental data, when the slip ratio was found from the expression of Zivi [39]. The theory did not agree with the experimental data when the vena-contracta phenomenon was assumed to occur.

6.2 Recommendation for future research

The experimental data obtained in this study make it clear that the conventional pressure drop calculation techniques are inadequate for mini and micro systems. The following recommendations are therefore made for future follow up research.

1. Experiments addressing flow area contraction and expansion ratios covering a reasonably wide range are recommended. In particular, experiments examining the pressure drop at the interface between a capillary and a large plenum are highly recommended.
2. Experiments are recommended in which liquids with different viscosities and surface tensions are used. Such experiments will elucidate the effects of the thermophysical fluid properties on the pressure drops associated with flow through abrupt flow area changes.
3. The experimental data thus far have addressed mini-channel systems. Experiments addressing flow area changes in microchannel size range (i.e., channels with $10\mu\text{m} \leq D_H \leq 100\mu\text{m}$) are highly recommended.

APPENDIX A

Data

Experimental data			Pressure drop along the channels (kPa)										
Water-expansion case													
\dot{m} (g/s)	Re	P_ref(kPa)	$\Delta P_{f,6}$	$\Delta P_{6,e}$	$\Delta P_{e,5}$	$\Delta P_{5,d}$	$\Delta P_{d,4}$	$\Delta P_{4,c}$	$\Delta P_{c,3}$	$\Delta P_{3,b}$	$\Delta P_{b,2}$	$\Delta P_{2,a}$	$\Delta P_{a,1}$
0.1032	159	96.8	0.5372	0.541	0.563	0.5544	0.551	0.5581	0.00138	0.00173	0.00107	0.00156	0.00176
0.1315	204	96.893	0.5647	0.5595	0.5905	0.5767	0.5682	0.5692	0.00296	0.00365	0.00417	0.00451	0.00387
0.1626	252	97.386	0.582	0.5784	0.606	0.5956	0.5905	0.5909	0.01053	0.00976	0.00984	0.01053	0.00977
0.1955	303	97.563	0.6077	0.5956	0.625	0.6146	0.6077	0.6079	0.0175	0.01689	0.01707	0.01741	0.01658
0.2273	352	97.84	0.6266	0.6232	0.6455	0.637	0.6266	0.6269	0.0227	0.02239	0.0234	0.02378	0.02257
0.2561	397	97.933	0.6576	0.649	0.6724	0.6736	0.6734	0.6738	0.0289	0.02921	0.02928	0.02962	0.02794
0.2865	444	98.022	0.68	0.6713	0.6765	0.6799	0.6868	0.687	0.0346	0.03401	0.03427	0.0347	0.03237
0.3175	492	98.431	0.704	0.6971	0.6937	0.6988	0.6954	0.6956	0.0382	0.03874	0.0378	0.0385	0.03669
0.3476	539	99.327	0.735	0.7298	0.7312	0.7401	0.7315	0.7318	0.0433	0.04242	0.04356	0.0444	0.04236
0.3806	593	100.019	0.7601	0.7592	0.7615	0.7613	0.7602	0.7605	0.04958	0.04944	0.04923	0.04975	0.04787
0.4238	632	100.523	0.7923	0.7919	0.7928	0.7915	0.7908	0.7909	0.0545	0.05487	0.05477	0.05508	0.05428

Experimental data Water-contraction		Total Pressure along the channels in (kPa)											
\dot{m} (g/s)	Re	P1(kPa)	P_A(kPa)	P2(kPa)	P_B(kPa)	P3(kPa)	P_C(kPa)	P4(kPa)	P_D(kPa)	P5(kPa)	P_E(kPa)	P6(kPa)	P_F(kPa)
0.1033	160	96.694	96.5593	96.4229	96.2899	96.1518	96.012	95.082	94.5414	93.9956	93.4508	92.9068	92.3809
0.1315	204	96.954	96.7815	96.6021	96.421	96.2468	96.0657	94.7984	94.2354	93.6742	93.1232	92.5619	92.0127
0.1626	252	97.06	96.8187	96.5757	96.3275	96.0776	95.8311	93.8561	93.2794	92.7001	92.132	91.5553	90.9837
0.1956	303	97.087	96.7949	96.5022	96.2107	95.9186	95.626	93.3303	92.7312	92.1356	91.5503	90.9529	90.3538
0.2273	353	97.137	96.7405	96.3385	95.9374	95.5387	95.1395	92.4953	91.8703	91.2453	90.6468	90.0569	89.4578
0.2561	397	97.16	96.6817	96.2039	95.7251	95.2469	94.7684	91.5996	90.8454	90.0944	89.3446	88.5939	87.8398
0.2865	442	97.231	96.6689	96.1058	95.543	94.9797	94.3528	91.1496	90.2639	89.3816	88.4965	87.8078	86.9207
0.3175	493	97.364	96.7384	96.112	95.4852	94.8589	94.232	90.6401	89.7344	88.8321	87.927	87.0216	86.1162
0.3476	539	97.723	97.0034	96.2841	95.5651	94.845	94.1252	90.2202	89.0776	87.9392	86.7995	85.6599	84.5201

Experimental data Air- Contraction				Pressure drop along the channels										
\dot{m} (g/s)	V(m/s)	Re	P_ref(kPa)	$\Delta P_{1,A}$	$\Delta P_{A,2}$	$\Delta P_{2,B}$	$\Delta P_{B,3}$	$\Delta P_{3,C}$	$\Delta P_{C,4}$	$\Delta P_{4,D}$	$\Delta P_{D,5}$	$\Delta P_{5,E}$	$\Delta P_{E,6}$	$\Delta P_{6,F}$
0.0243	35.5	1997	0.04208	0.0265	0.0193	0.0287	0.0262	0.0224	1.4264	0.5277	0.4689	0.4419	0.4265	0.4261
0.0377	55.2	3103	0.0952	0.0534	0.0355	0.0479	0.0355	0.0423	3.0569	1.0132	0.8474	1.3406	1.4044	1.4484
0.0505	73.8	4153	0.14827	0.0846	0.0784	0.1081	0.0942	0.0919	5.7261	4.3436	2.6343	2.4853	2.7181	2.5867
0.0627	92.1	5181	0.2014	1.1484	0.1397	0.1665	0.1573	0.1462	6.5456	6.0144	4.0945	3.8468	4.3436	4.1855
0.0746	108.1	6130	0.2545	0.2026	0.1868	0.2229	0.2214	0.1981	9.8123	7.9131	5.8739	5.2463	6.2663	5.9284
0.0846	123.6	6953	0.3606	0.2523	0.2394	0.2839	0.2705	0.2478	10.2842	9.7855	7.5925	6.8042	8.2327	7.9533
0.0937	136.9	7701	0.4137	0.2997	0.2983	0.3405	0.3318	0.3042	10.4625	10.1013	9.5164	8.4755	10.0179	9.8552
0.1023	149.5	8408	0.511	0.3448	0.3845	0.4035	0.3909	0.3561	10.5533	10.6206	10.2613	9.3121	10.4262	10.4625
0.1099	160.6	9035	0.6261	0.3855	0.3855	0.4575	0.4487	0.4058	10.6453	10.7141	10.4625	9.9653	10.5675	10.5459
0.1196	174.8	9830	0.7323	0.4487	0.4679	0.5458	0.5277	0.4893	10.7101	10.6423	10.5981	10.4217	10.6143	10.6743
0.1266	185.1	10409	0.8385	0.4938	0.4862	0.5977	0.5703	0.5345	10.7343	10.6675	10.6432	10.5016	10.6069	10.6848
0.1334	195.6	11002	0.9978	0.5323	0.5995	0.6587	0.6045	0.5842	10.7156	10.7561	10.7311	10.6423	10.7011	10.7291

Experimental Data		Pressure drop along the channels (kPa)											
Air-expansion													
\dot{m} (g/s)	Re	P_ref(kPa)	$\Delta P_{F,6}$	$\Delta P_{6,E}$	$\Delta P_{E,5}$	$\Delta P_{5,D}$	$\Delta P_{D,4}$	$\Delta P_{4,C}$	$\Delta P_{C,3}$	$\Delta P_{3,B}$	$\Delta P_{B,2}$	$\Delta P_{2,A}$	$\Delta P_{A,1}$
0.0243	35.5	0.1483	0.0152	0.0287	0.0298	0.0384	0.0365	0.0455	0.0087	0.0092	0.0088	0.0084	0.0089
0.0377	55.2	0.4668	0.0423	0.0536	0.0521	0.0747	0.0518	0.0798	0.0223	0.0101	0.0123	0.0102	0.0061
0.0505	73.8	0.6792	0.0761	0.0897	0.0828	0.0865	0.0877	0.0881	0.0347	0.0392	0.0345	0.0312	0.0084
0.0627	92.1	0.9447	0.1145	0.1281	0.1559	0.1378	0.1286	0.1752	0.0467	0.0618	0.0466	0.0456	0.0177
0.0746	108.1	1.2102	0.1552	0.1755	0.1743	0.1585	0.1423	0.1836	0.0618	0.0618	0.0844	0.0626	0.0312
0.0846	123.6	1.4756	0.2071	0.2342	0.2077	0.2384	0.2607	0.2949	0.0429	0.0618	0.0521	0.0429	0.0462
0.0937	136.9	1.7411	0.2726	0.3019	0.2439	0.2101	0.2825	0.3371	0.0197	0.0084	0.0642	0.0623	0.0614
0.1023	149.5	2.0549	0.3384	0.3764	0.3418	0.3371	0.3078	0.3513	0.0914	0.0906	0.0977	0.1484	0.0998
0.1099	160.6	2.3251	0.3499	0.4546	0.4162	0.4687	0.4371	0.4774	0.1553	0.1295	0.1408	0.1245	0.1197
0.1196	174.8	2.8303	0.5164	0.6158	0.5726	0.5648	0.5823	0.5926	0.4005	0.1295	0.1671	0.1545	0.1597
0.1266	185.1	3.1746	0.6067	0.7422	0.6155	0.6748	0.7071	0.8652	0.0446	0.0151	0.2843	0.2929	0.1868
0.1334	195.6	3.5346	0.7084	0.8763	0.7606	0.8358	0.8326	0.9935	0.2536	0.2249	0.2597	0.2261	0.2166

Two-phase Contraction Data

Re_L=444

Re_g=570 - 2031

m_dotLg	m_dot_L	Re_g	P_1(kPa)	P_A	P2	P_B	P3	P_c	P4	P_D	P5	P_E	P6	P_F
0.0068	0.2865	570	99.69	99.4859	99.2621	99.0386	98.8142	98.5908	97.7277	96.8689	96.0114	95.1528	94.2934	93.4141
0.0093	0.2865	776	99.944	99.5341	99.1363	98.735	98.3268	97.9217	96.91012	95.89862	94.88762	93.87692	92.86603	91.85497
0.0115	0.2865	963	100.222	99.6453	99.0823	98.509	97.9288	97.3572	96.0896	94.8228	93.5557	92.2882	91.0209	89.7539
0.0161	0.2865	1342	101.096	100.3989	99.7049	99.0136	98.3239	97.7162	96.2416	94.7674	93.293	91.8193	90.3454	88.8717
0.0205	0.2865	1712	101.839	100.9045	99.9666	99.0352	98.11014	97.18594	95.01684	92.84894	90.68084	88.51264	86.34454	84.17614
0.0244	0.2865	2031	102.9	101.7832	100.6561	99.5531	98.4397	97.3281	94.6361	91.9503	89.264	86.5775	83.8905	81.204

Re_L=397

Re_g=570 - 2444

m_dotLg	m_dot_L	Re_g	P_1(kPa)	P_A	P2	P_B	P3	P_c	P4	P_D	P5	P_E	P6	P_F
0.0093	0.2561	570	99.465	99.3131	99.1733	99.018	98.8592	98.6936	96.8219	94.9521	93.0819	91.2203	89.3503	87.4807
0.0139	0.2561	1158	99.848	99.562	99.2691	98.9813	98.6892	98.3996	96.4077	94.4178	92.4278	90.4376	88.4481	86.4582
0.0183	0.2561	1532	100.034	99.619	99.2005	98.7889	98.367	97.9537	95.4098	92.8673	90.3251	87.7828	85.2406	82.6986
0.0225	0.2561	1876	100.737	100.2205	99.7143	99.2029	98.6847	98.1737	95.2378	92.3035	89.3688	86.4348	83.501	80.5669
0.0261	0.2561	2178	100.926	100.2323	99.5403	98.838	98.1409	97.4441	93.6964	89.9506	86.2046	82.4584	78.7128	74.9668
0.0293	0.2561	2444	101.763	100.559	99.36	98.154	96.9529	95.7527	91.5316	87.3126	83.0936	78.8748	74.6562	70.4372

Re_L=539
 Re_g=570 - 2317

m_dotLg	m_dot_L	Re_g	P_1(kPa)	P_A	P2	P_B	P3	P_c	P4	P_D	P5	P_E	P6	P_F
0.0068	0.6288	570	99.79	99.3182	98.8516	98.3764	97.9108	97.4364	95.5803	93.7291	91.871	90.0284	88.1754	86.3336
0.0093	0.6288	776	100.716	100.1823	99.6537	99.1269	98.5914	98.0637	95.4042	93.2726	91.1496	89.0283	86.8932	84.7685
0.0115	0.6288	964	101.125	100.5259	99.9337	99.3243	98.7158	98.11	94.4149	91.4319	88.4484	85.469	82.481	79.4985
0.0161	0.6288	1341	101.798	100.9186	100.0443	99.1664	98.3028	97.4395	93.1075	89.9157	86.7177	83.5268	80.3302	77.1377
0.0205	0.6288	1712	103.022	101.9654	100.9036	99.8458	98.7894	97.7302	92.1552	88.1419	84.1217	80.1088	76.0919	72.0803
0.0244	0.6288	2031	105.129	103.8282	102.5299	101.2287	99.9265	98.626	92.1961	87.9522	83.7098	79.4647	75.2204	70.9774
0.0278	0.6288	1317	105.975	104.317	102.652	100.993	99.3351	97.6786	90.1961	85.8299	81.47	77.1043	72.7455	68.3855

Re_L=303
 Re_g=570 - 2031

m_dotLg	m_dot_L	Re_g	P_1(kPa)	P_A	P2	P_B	P3	P_c	P4	P_D	P5	P_E	P6	P_F
0.0068	0.1955	570	98.849	98.4575	98.0647	97.6734	97.2816	96.8905	95.9409	95.2084	94.4753	93.7428	93.0109	92.2794
0.0093	0.1955	776	99.273	98.8406	98.4039	97.9656	97.5285	97.0911	95.5973	94.7478	93.8971	93.0488	92.1981	91.3496
0.0115	0.1955	964	99.454	98.9886	98.5258	98.0623	97.5929	97.1242	94.8849	94	93.1135	92.2298	91.3438	90.4604
0.0161	0.1955	1341	99.596	99.0355	98.4762	97.9162	97.3553	96.7965	93.7882	92.3993	91.0089	89.6319	88.2382	86.86
0.0205	0.1955	1721	100.209	99.6094	99.0102	98.4113	97.8108	97.2104	93.5122	91.5942	89.6755	87.7592	85.84	83.9229
0.0244	0.1955	2031	100.659	99.9903	99.3221	98.6472	97.9724	97.3032	92.953	90.7211	88.4887	86.2575	84.0251	81.7948

Two-phase - Expansion Data

Re_L=492 Re_g=1425	P_ref(kPa)	P_F-P6	P6-P_E	P_E-P5	P5-P_D	P_D-P4	P4-P_c	P_c-P3	P3-P_B	P_B-P2	P2-P_A	P_A-P1
	101.839	0.4821	0.4477	0.4873	0.4701	0.4942	2.416	1.2362	0.9465	1.0131	0.993	0.915
	P_F(kPa)	P6	P_E	P5	P_D	P4	P_c	P3	P_B	P2	P_A	P1
	101.839	101.3569	100.9092	100.4219	99.9518	99.4576	97.0416	95.8054	94.8589	93.8458	92.8528	91.9378
Re_L=492 Re_g=2025	P_ref(kPa)	P_F-P6	P6-P_E	P_E-P5	P5-P_D	P_D-P4	P4-P_c	P_c-P3	P3-P_B	P_B-P2	P2-P_A	P_A-P1
	102.677	0.563	0.5432	0.5344	0.5423	0.5337	1.1581	1.1185	1.1308	1.2564	1.2215	1.2008
	P_F(kPa)	P6	P_E	P5	P_D	P4	P_c	P3	P_B	P2	P_A	P1
	102.677	102.114	101.5708	101.0364	100.4941	99.9604	98.8023	97.6838	96.553	95.2966	94.0751	92.8743
Re_L=492 Re_g=2608	P_ref(kPa)	P_F-P6	P6-P_E	P_E-P5	P5-P_D	P_D-P4	P4-P_c	P_c-P3	P3-P_B	P_B-P2	P2-P_A	P_A-P1
	103.795	0.821	0.929	0.8278	0.8382	0.8264	1.6913	1.7687	1.7806	1.8121	1.8165	1.7928
	P_F(kPa)	P6	P_E	P5	P_D	P4	P_c	P3	P_B	P2	P_A	P1
	103.795	102.974	102.045	101.2172	100.379	99.5526	97.8613	96.0926	94.312	92.4999	90.6834	88.8906
Re_L=492 Re_g=3141	P_ref(kPa)	P_F-P6	P6-P_E	P_E-P5	P5-P_D	P_D-P4	P4-P_c	P_c-P3	P3-P_B	P_B-P2	P2-P_A	P_A-P1
	106.592	0.9792	0.9964	0.9775	0.9912	0.9844	2.0181	2.037	2.0318	2.049	2.0642	2.0231
	P_F(kPa)	P6	P_E	P5	P_D	P4	P_c	P3	P_B	P2	P_A	P1
	106.592	105.6128	104.6164	103.6389	102.6477	101.6633	99.6452	97.6082	95.5764	93.5274	91.4632	89.4401
Re_L=492 Re_g=3683	P_ref(kPa)	P_F-P6	P6-P_E	P_E-P5	P5-P_D	P_D-P4	P4-P_c	P_c-P3	P3-P_B	P_B-P2	P2-P_A	P_A-P1
	108.901	1.079	1.0927	1.0893	1.103	1.0735	2.4343	2.3019	2.467	2.479	2.3243	2.4137
	P_F(kPa)	P6	P_E	P5	P_D	P4	P_c	P3	P_B	P2	P_A	P1
	108.901	107.822	106.7293	105.64	104.537	103.4635	101.0292	98.7273	96.2603	93.7813	91.457	89.0433
Re_L=492 Re_g=4208	P_ref(kPa)	P_F-P6	P6-P_E	P_E-P5	P5-P_D	P_D-P4	P4-P_c	P_c-P3	P3-P_B	P_B-P2	P2-P_A	P_A-P1
	109.444	1.2028	1.2114	1.22	1.1959	1.2062	2.6906	2.6992	2.7078	2.713	2.7009	2.7198
	P_F(kPa)	P6	P_E	P5	P_D	P4	P_c	P3	P_B	P2	P_A	P1
	109.444	108.2412	107.0298	105.8098	104.6139	103.4077	100.7171	98.0179	95.3101	92.5971	89.8962	87.1764

Re_L=397												
Re_g=2025	P_ref(kPa)	P_F-P6	P6-P_E	P_E-P5	P5-P_D	P_D-P4	P4-P_c	P_c-P3	P3-P_B	P_B-P2	P2-P_A	P_A-P1
	101.12	1.062	1.1254	1.065	1.1581	1.1014	1.8237	1.7979	1.7893	1.8103	1.8117	1.0814
	P_F(kPa)	P6	P_E	P5	P_D	P4	P_c	P3	P_B	P2	P_A	P1
	101.12	100.058	98.9326	97.8676	96.7095	95.6081	93.7844	91.9865	90.1972	88.3869	86.5752	85.4938
Re_L=397												
Re_g=2608	P_ref(kPa)	P_F-P6	P6-P_E	P_E-P5	P5-P_D	P_D-P4	P4-P_c	P_c-P3	P3-P_B	P_B-P2	P2-P_A	P_A-P1
	102.584	1.8306	1.8151	1.8065	1.7928	1.8272	2.5117	2.5083	2.4945	2.479	2.5152	2.5066
	P_F(kPa)	P6	P_E	P5	P_D	P4	P_c	P3	P_B	P2	P_A	P1
	102.584	100.7534	98.9383	97.1318	95.339	93.5118	91.0001	88.4918	85.9973	83.5183	81.0031	78.4965
Re_L=397												
Re_g=3141	P_ref(kPa)	P_F-P6	P6-P_E	P_E-P5	P5-P_D	P_D-P4	P4-P_c	P_c-P3	P3-P_B	P_B-P2	P2-P_A	P_A-P1
	104.762	2.2916	2.2761	2.2881	2.295	2.3105	2.9882	3.0226	3.0071	3.0105	3.0152	3.0123
	P_F(kPa)	P6	P_E	P5	P_D	P4	P_c	P3	P_B	P2	P_A	P1
	104.762	102.4704	100.1943	97.9062	95.6112	93.3007	90.3125	87.2899	84.2828	81.2723	78.2571	75.2448
Re_L=397												
Re_g=3683	P_ref(kPa)	P_F-P6	P6-P_E	P_E-P5	P5-P_D	P_D-P4	P4-P_c	P_c-P3	P3-P_B	P_B-P2	P2-P_A	P_A-P1
	107.232	2.8179	2.8093	2.8248	2.8334	2.8231	3.4921	3.5317	3.5059	3.4956	3.5334	3.5214
	P_F(kPa)	P6	P_E	P5	P_D	P4	P_c	P3	P_B	P2	P_A	P1
	107.232	104.4141	101.6048	98.78	95.9466	93.1235	89.6314	86.0997	82.5938	79.0982	75.5648	72.0434
Re_L=397												
Re_g=4208	P_ref(kPa)	P_F-P6	P6-P_E	P_E-P5	P5-P_D	P_D-P4	P4-P_c	P_c-P3	P3-P_B	P_B-P2	P2-P_A	P_A-P1
	108.32	3.1137	3.1189	3.1086	3.1258	3.102	3.872	3.9428	3.9084	3.9393	3.9514	3.9135
	P_F(kPa)	P6	P_E	P5	P_D	P4	P_c	P3	P_B	P2	P_A	P1
	108.32	105.2063	102.0874	98.9788	95.853	92.751	88.879	84.9362	81.0278	77.0885	73.1371	69.2236
Re_L=397												
Re_g=4733	P_ref(kPa)	P_F-P6	P6-P_E	P_E-P5	P5-P_D	P_D-P4	P4-P_c	P_c-P3	P3-P_B	P_B-P2	P2-P_A	P_A-P1
	108.978	3.565	3.5833	3.5919	3.5886	4.0253	4.0322	4.0133	4.0219	4.0305	4.0253	4.0228
	P_F(kPa)	P6	P_E	P5	P_D	P4	P_c	P3	P_B	P2	P_A	P1
	108.978	105.413	101.8297	98.2378	94.6492	90.6239	86.5917	82.5784	78.5565	74.526	70.5007	66.4779

Re_L=444												
Re_g=2316	P_ref(kPa)	P_F-P6	P6-P_E	P_E-P5	P5-P_D	P_D-P4	P4-P_c	P_c-P3	P3-P_B	P_B-P2	P2-P_A	P_A-P1
	101.158	2.0336	2.0318	2.037	2.0302	2.0336	2.5582	2.5478	2.5513	2.5599	2.5547	2.5599
	P_F(kPa)	P6	P_E	P5	P_D	P4	P_c	P3	P_B	P2	P_A	P1
	101.158	99.1244	97.0926	95.0556	93.0254	90.9918	88.4336	85.8858	83.3345	80.7746	78.2199	75.66
Re_L=444												
Re_g=2883	P_ref(kPa)	P_F-P6	P6-P_E	P_E-P5	P5-P_D	P_D-P4	P4-P_c	P_c-P3	P3-P_B	P_B-P2	P2-P_A	P_A-P1
	103.172	2.351	2.3415	2.3535	2.3601	2.3552	2.8695	2.8574	2.854	2.8626	2.8712	2.8678
	P_F(kPa)	P6	P_E	P5	P_D	P4	P_c	P3	P_B	P2	P_A	P1
	103.172	100.821	98.4795	96.126	93.7659	91.4107	88.5412	85.6838	82.8298	79.9672	77.096	74.2282
Re_L=444												
Re_g=3416	P_ref(kPa)	P_F-P6	P6-P_E	P_E-P5	P5-P_D	P_D-P4	P4-P_c	P_c-P3	P3-P_B	P_B-P2	P2-P_A	P_A-P1
	105.877	2.558	2.551	2.556	2.556	2.5478	3.1739	3.1997	3.1894	3.1825	3.2032	3.1997
	P_F(kPa)	P6	P_E	P5	P_D	P4	P_c	P3	P_B	P2	P_A	P1
	105.877	103.319	100.768	98.212	95.656	93.1082	89.9343	86.7346	83.5452	80.3627	77.1595	73.9598
Re_L=444												
Re_g=3949	P_ref(kPa)	P_F-P6	P6-P_E	P_E-P5	P5-P_D	P_D-P4	P4-P_c	P_c-P3	P3-P_B	P_B-P2	P2-P_A	P_A-P1
	107.798	2.8933	2.9157	2.9007	2.902	2.9105	3.6192	3.5985	3.5934	3.5899	3.5976	3.597
	P_F(kPa)	P6	P_E	P5	P_D	P4	P_c	P3	P_B	P2	P_A	P1
	107.798	104.9047	101.989	99.0883	96.1863	93.2758	89.6566	86.0581	82.4647	78.8748	75.2772	71.6802
Re_L=444												
Re_g=4466	P_ref(kPa)	P_F-P6	P6-P_E	P_E-P5	P5-P_D	P_D-P4	P4-P_c	P_c-P3	P3-P_B	P_B-P2	P2-P_A	P_A-P1
	109.888	3.2668	3.2565	3.2702	3.2737	3.2806	3.9569	3.9621	3.9846	3.9541	3.9538	3.9533
	P_F(kPa)	P6	P_E	P5	P_D	P4	P_c	P3	P_B	P2	P_A	P1
	109.888	106.6212	103.3647	100.0945	96.8208	93.5402	89.5833	85.6212	81.6366	77.6825	73.7287	69.7754

Re_L=492												
Re_g=775	P_ref(kPa)	P_F-P6	P6-P_E	P_E-P5	P5-P_D	P_D-P4	P4-P_c	P_c-P3	P3-P_B	P_B-P2	P2-P_A	P_A-P1
	99.1975	2.242	2.2439	2.2393	2.2415	2.2398	2.6163	0.6847	0.6842	0.6937	0.6971	0.692
	P_F(kPa)	P6	P_E	P5	P_D	P4	P_c	P3	P_B	P2	P_A	P1
	99.1975	96.9555	94.7116	92.4723	90.2308	87.991	85.3747	84.69	84.0058	83.3121	82.615	81.923
Re_L=492												
Re_g=958	P_ref(kPa)	P_F-P6	P6-P_E	P_E-P5	P5-P_D	P_D-P4	P4-P_c	P_c-P3	P3-P_B	P_B-P2	P2-P_A	P_A-P1
	99.541	2.4223	2.4214	2.4243	2.4231	2.4259	2.8574	0.9157	0.9166	0.9173	0.9166	0.9156
	P_F(kPa)	P6	P_E	P5	P_D	P4	P_c	P3	P_B	P2	P_A	P1
	99.541	97.1187	94.6973	92.273	89.8499	87.424	84.5666	83.6509	82.7343	81.817	80.9004	79.9848
Re_L=492												
Re_g=1158	P_ref(kPa)	P_F-P6	P6-P_E	P_E-P5	P5-P_D	P_D-P4	P4-P_c	P_c-P3	P3-P_B	P_B-P2	P2-P_A	P_A-P1
	99.92	2.5771	2.5659	2.5692	2.5711	2.575	3.2885	1.2338	1.2234	1.2303	1.2363	1.2296
	P_F(kPa)	P6	P_E	P5	P_D	P4	P_c	P3	P_B	P2	P_A	P1
	99.92	97.3429	94.777	92.2078	89.6367	87.0617	83.7732	82.5394	81.316	80.0857	78.8494	77.6198
Re_L=492												
Re_g=1341	P_ref(kPa)	P_F-P6	P6-P_E	P_E-P5	P5-P_D	P_D-P4	P4-P_c	P_c-P3	P3-P_B	P_B-P2	P2-P_A	P_A-P1
	100.322	2.6837	2.6854	2.6958	2.7026	2.7061	3.6956	1.3593	1.356	1.3545	1.3553	1.356
	P_F(kPa)	P6	P_E	P5	P_D	P4	P_c	P3	P_B	P2	P_A	P1
	100.322	97.6383	94.9529	92.2571	89.5545	86.8484	83.1528	81.7935	80.4375	79.083	77.7277	76.3717
Re_L=492												
Re_g=1533	P_ref(kPa)	P_F-P6	P6-P_E	P_E-P5	P5-P_D	P_D-P4	P4-P_c	P_c-P3	P3-P_B	P_B-P2	P2-P_A	P_A-P1
	100.538	2.9727	2.9725	2.9713	2.9718	2.9732	3.9677	1.7116	1.71	1.7107	1.7111	1.7102
	P_F(kPa)	P6	P_E	P5	P_D	P4	P_c	P3	P_B	P2	P_A	P1
	100.538	97.5653	94.5928	91.6215	88.6497	85.6765	81.7088	79.9972	78.2872	76.5765	74.8654	73.1552
Re_L=492												
Re_g=1875	P_ref(kPa)	P_F-P6	P6-P_E	P_E-P5	P5-P_D	P_D-P4	P4-P_c	P_c-P3	P3-P_B	P_B-P2	P2-P_A	P_A-P1
	101.711	3.3322	3.3313	3.3303	3.3321	3.333	4.358	2.1476	2.1435	2.1464	2.1466	2.1445
	P_F(kPa)	P6	P_E	P5	P_D	P4	P_c	P3	P_B	P2	P_A	P1
	101.711	98.3788	95.0475	91.7172	88.3851	85.0521	80.6941	78.5465	76.403	74.2566	72.11	69.9655
Re_L=492												
Re_g=2173	P_ref(kPa)	P_F-P6	P6-P_E	P_E-P5	P5-P_D	P_D-P4	P4-P_c	P_c-P3	P3-P_B	P_B-P2	P2-P_A	P_A-P1
	102.647	3.8368	3.8411	3.8397	3.8387	3.8404	4.7866	2.564	2.5492	2.556	2.5613	2.5511
	P_F(kPa)	P6	P_E	P5	P_D	P4	P_c	P3	P_B	P2	P_A	P1
	102.647	98.8102	94.9691	91.1294	87.2907	83.4503	78.6637	76.0997	73.5505	70.9945	68.4332	65.8821

BIBLIOGRAPHY

- [1] S.M. Ghiaasiaan, S.I. Abdel-Khalik, Two-phase flow in micro-channels, *Adv. Heat Transfer* 34 (2001) 145-254.
- [2] S.G. Kandlikar, Fundamental issues related to flow boiling in minichannels and microchannels. *Exp. Thermal and Fluid Science*, 26 (2002) 389-407.
- [3] F.F. Abdelall, G. Hahn, S.M. Ghiaasiaan, S.I. Abdel-Khalik, S.S. Jeter, M. Yoda, D.L. Sadowski, Pressure drop caused by abrupt flow area changes in small channels, *Exp. Thermal and Fluid Science* 29 (2005) 425-434.
- [4] E. Guyon, J-P. Hulin et L. Petit, *Hydrodynamique Physique*, Inter-editions/ Editions du CNRS, Paris (1991).
- [5] R.B. Bird, W.E. Stewart et E.N. Lightfoot, *Transport Phenomena*, John Wiley & Sons, New York (1960).
- [6] M. Gad-el-Hak, The Fluid Mechanics of Microdevices, *J. of Fluid Engineering*, 121 (1999) 7-33.
- [7] Moore, G.E., Cramming More Components onto Integrated Circuits, *Electronics*, Vol. 38, No. 8, April 19, 1965
- [8] Hetsroni, G.; Mosyak, A.; Pogrebnyak, E.; and Yarin, L.P., Fluid Flow in Microchannels, *International Journal of Heat and Mass Transfer*, Vol. 48 (2005), pp. 1982-1998.
- [9] M.J. Kohl, S.I. Abdel-Khalik, S.M. Jeter, D.L. Sadowski, An experimental investigation of microchannel flow with internal pressure measurements. *Int. J. Heat and Mass Transfer* 48 (2005) 1518-1533.
- [10] M.J. Kohl, S.I. Abdel-Khalik, S.M. Jeter, D.L. Sadowski, A microfluidic experimental platform with internal pressure measurements. *Sensors and Actuators A* 118 (2005) 212-221.
- [11] D.B. Tuckerman, R.F.W. Pease, high performance heat sinking for VLSI, *IEEE Electron. Device Lett.* EDL2 (1982) 126-129.
- [12] P. Bradshaw, F.Y.F. Wong, The reattachment and relaxation of a turbulent shear layer, *J. Fluid Mech.* 52 (1972) 113-135.
- [13] J.C. Shih, C.-M. Ho, Y.-C. Tai, Monatomic and polyatomic gas flow through uniform microchannels, *Proc. ASME DSC* 59 (1996) 197-203.

- [14] I. Papautsky, J. Brazzle, Laminar fluid behavior in microchannels using micropolar fluid theory, *Sensors and Actuators* 73 (1999) 101-108.
- [15] W. Urbanck, J. Zemel, H. Bau, An investigation of the temperature dependence of Poiseuille number in micro-channel flow, *J. Micromech. Microeng.* 3 (1993) 206-208
- [16] J. Judy, D. Maynes, B. Webb, Characterization of frictional pressure drop for liquid flows through micro-channels, *Int. J. Heat Mass Transfer* 45 (17) (2002) 3477-3489.
- [17] T. Bayraktar, S.B. Pidugu, Characterization of liquid flows in microfluidic systems. *Int. J. Heat and Mass Transfer* 49 (2006) 815-824.
- [18] O.J. Mendler, A.S. Rathbun, N.E. Vanhuff, A. Weiss, Natural-circulation tests with water at 800 to 2000 psia under non boiling, local boiling and bulk boiling conditions. *J. Heat Transfer, ASME*, 83 C (3), (1961) 261-273.
- [19] A. Attou, L. Bolle, Evaluation of the Two-phase pressure loss across singularities, FED-Vol. 210, *Cavitation and Multiphase Flow*, ASME 1995.
- [20] D. Chisholm, L.A. Sutherland, Prediction of pressure gradients in pipeline systems during two-phase flow. *Proceedings of the Institution of Mechanical Engineers*, 1969, 184, Pt 3C, 24-32.
- [21] I. Velasco, L'écoulement diphasique a travers un élargissement brusque. *Travail de maitrise, Universite catholique de Louvain*, 1975.
- [22] M. Wadle, A new formula for the pressure recovery in an abrupt diffuser. *International Journal of Multiphase Flow*, 1989, 15, 241-256.
- [23] I. Owen, A. Abdou-Ghani, A.M. Amini, Diffusing a homogenized two-phase flow. *International Journal of Multiphase Flow*, 1992, 18, 531-540.
- [24] J. Schmidt, L. Friedel, Two-phase pressure drop across sudden contraction in duct areas, *Int. J. Multiphase Flow*, Vol. 23, No.2, pp. 283-299, 1997.
- [25] W.M. Kays, Loss coefficient for abrupt changes in flow cross section with low Reynolds number flow in single and multiple tube systems, *Trans. ASME* 72 (1950) 1067-1074.
- [26] G.E. Geiger, Sudden Contraction Losses in Single and Two-phase Flow, Ph.D. Thesis, University of Pittsburgh, 1964.
- [27] T.R. Lahey Jr., F.J. Moody, *The Thermal Hydraulics of Boiling Water Nuclear Reactors*, second ed., American Nuclear Society, LaGrange Park, IL, 1993.

- [28] J.G. Collier, J.R. Thome, *Convective Boiling and Condensation*, Clarendon Press, Oxford, 1994.
- [29] J. Weisman, A. Hussain, B. Harshe, Two phase pressure drop across abrupt area changes and restrictions, in: T.N. Veziroglu, S. Kakac (Eds), *Proc. Two-Phase and Heat Transfer Symposium*, Hemisphere, Washington, DC, 1976, pp. 301-303.
- [30] E. Jansen, J.A. Kervinen, Two-phase pressure drop across contraction and expansion, steam-water mixture at 600-1400 psia, Report GEAP-4622, 1964.
- [31] G. Gnnglielmini, A. Lorenzi, A. Muzzio, G. Sotgia, Two-phase flow pressure drops across sudden area contractions pressure and void fraction profiles, in: *Proc. 8th Int. Heat Transfer Conf.*, 1986, vol. 5, 2361-2366.
- [32] D. Chisholm, Prediction of pressure losses of changes of section, bends and throttling devices, NEL Report 388, 1968.
- [33] N.S. AI'Ferov, Ye.N. Shul'Zhenko, Pressure drops in two-phase flows through local resistances, *Fluid Mech.-Sov. Res.* 6 (1977) 20-33.
- [34] A. Attou, M. Giot, J.M. Seynhaeven, Modeling of steady-state two-phase bubbly flow through a sudden enlargement, *Int. J. Heat Mass Transfer* 40 (1997) 3375-3385.
- [35] S.M. Zivi, Estimation of steady state steam void-fraction by means of principle of minimum entropy production, *ASME Trans. Series C* 86 (1964) 237-252.
- [36] A. Premoli, D. Francesco, and A. Prina, An empirical correlation for evaluating two-phase mixture density under adiabatic conditions, *European Two-Phase Flow Group Meeting*, Milan (1970)
- [37] K. Mishima, T. Hibiki, Some characteristics of air-water two-phase flow in small diameter vertical tube. *Int. J. Multiphase Flow*, 22 (1996) 703-712.
- [38] A.A. Armand, The resistance during the movement of a two-phase system in horizontal pipes. *AERE Libr. Trans.* Vol. 828 (1959).